Response to Reviewer #1's Comments

Anonymous Referee #1:

The authors presented a set of valuable data and conducted a meaningful analysis of the data. I have a few comments, which may help improve clarity in some places. I don't view that it is reviewers' responsibility to copy-edit and hence I did not point out all grammatical errors, but the manuscript needs careful editing.

We sincerely appreciate the reviewer's valuable comments and helpful suggestions on this manuscript. We have carefully checked the grammar, syntax and semantic of all languages throughout the manuscript based on the reviewer's suggestions. We have responded to all the comments point-by-point and made corresponding changes in the revised manuscript as highlighted in red color. Please check the detailed responses to all the comments as below. The reviewer's comments are in black and our replies are in blue.

(1) Some of the results need to be quantitative. For instance, in the abstract, how much higher were GEM and RGM concentrations in the northern SCS, Hgp2.5 and Hgp10 in PRE than other areas (lines 48 -50)? How much higher were RGM concentrations during the day than at night (lines 54 -56)? How much higher were their GEM concentrations than "those background sites in the southern hemisphere" (lines 232-233) and "remote oceans" (lines 234-235)? How much higher were the GEM concentrations over the northern SCS from a previous studies (lines 238-240)? They need to be quantitative about such comparisons.

Response:

We agree with the reviewer that the results should be quantitative. The concrete data has been added in the revised manuscript.

See the revised manuscript at lines 19-29, 210-218, 295, 422-423, 427-428.

(2) Lines 81 – 88: Ye et al. (2016, acp) would be a good reference to cite, because their box model included the most up-to-date gas-phase reactions of Hg and Br and simulated contributions from variation oxidation reactions to GEM oxidation.

Response:

Thanks for the reviewer's suggestions. We have made a careful study on the paper of "Investigation of processes controlling summertime gaseous elemental mercury oxidation at midlatitudinal marine, coastal, and inland sites". The reference has been added in the revised manuscript (lines 57-59, 62-65, 91, 750-752).

Reference:

Ye, Z., Mao, H., Lin, C.-J., and Kim, S. Y.: Investigation of processes controlling summertime gaseous elemental mercury oxidation at midlatitudinal marine, coastal, and inland sites, Atmos. Chem. Phys., 16, 8461–8478, https://doi.org/10.5194/acp-16-8461-2016, 2016.

(3) Line 97 – 102: Grammatical errors. They might want to break this rambling passage to three sentences.

Response:

Thanks for your suggestion. This sentence has been divided into three sentences, which has been revised as "The atmospheric reactive Hg deposited to the oceans follows different reaction pathways. One important process is that divalent Hg can be combined with the

existing particles followed by sedimentation, or be converted to methylmercury (MeHg), the most bioaccumulative and toxic form of Hg in seafood (Ahn et al., 2010; Mason et al., 2017). Another important process is that the divalent Hg can be converted to dissolved gaseous Hg (DGM) through abiotic and biotic mechanisms (Strode et al., 2007)." in the revised manuscript.

Moreover, a section heading (3.5 Relationship between atmospheric Hg and meteorological parameters) has been added in the revised manuscript to make the structure of the manuscript clearer.

See the revised manuscript at lines 74-79, 401, 421.

(4) Lines 103 – 108: Too many excess articles. In fact, this was fairly commonly throughout the text. They might want to give it a good editing to get rid of those excess articles.
Response:
Thanks for the suggestion. We have checked all the references throughout the manuscript, and deleted those old and weakly related articles.

(5) Line 115: Mao et al. (2016, acp) provided a fairly complete review of the literature, up to early 2016, on spatiotemporal distributions of GEM, GOM, and PBM in different environments worldwide, including coastal areas. Not just these four studies for reference.
Response:
Thanks for your comments. We have read carefully the paper of "Current understanding of the driving mechanisms for spatiotemporal variations of atmospheric speciated mercury: a review". The related references (Ye et al., 2016 and Mao et al., 2016, 2017) have been added in the revised manuscript.
See the revised manuscript at lines 91-92.
References:
1) Ye, Z., Mao, H., Lin, C.-J., and Kim, S. Y.: Investigation of processes controlling summertime gaseous elemental mercury oxidation at midlatitudinal marine, coastal, and inland sites, Atmos. Chem. Phys., 16, 8461−8478, https://doi.org/10.5194/acp-16-8461-2016, 2016.
2) Mao, H., Cheng, I., and Zhang, L.: Current understanding of the driving mechanisms for spatiotemporal variations of atmospheric speciated mercury: a review, Atmos. Chem. Phys., 16, 12897−12924, https://doi.org/10.5194/acp-16-12897-2016, 2016.
3) Mao, H., Hall, D., Ye, Z., Zhou, Y., Felton, D., and Zhang, L.: Impacts of large-scale circulation on urban ambient concentrations of gaseous elemental mercury in New York, USA, Atmos. Chem. Phys., 17, 11655−11671, https://doi.org/10.5194/acp-17-11655-2017, 2017.

(6) Lines 258-259: The larger variabilities in RGM and Hgp were due not only to scavenging but also likely due to their sensitivity to meteorological conditions and chemical environments.
Response:
Thanks for the insightful comments and we do agree with the reviewer's comments. Thus, this sentence has been revised as "indicating that atmospheric reactive Hg was easily scavenged from the marine atmosphere due not only to their characteristics (high activity and solubility) but also due to their sensitivity to meteorological conditions and chemical environments" in the revised manuscript.

See the revised manuscript at lines 237-239.

(7) Figure 3a: I suggest that the lines be thickened to make it clearer. Please indicate where PRE is on the map. Every reader does not necessarily know where PRE is.

Response: Thanks for your suggestions. The lines have been thickened in the Figure 3a (see the revised manuscript at line 770) and Figures S2 and S3 (see the revised supplement at lines 60, 62). The location of the Pearl River Estuary (PRE) has been marked in Figures 1 and 3a (see lines 758, 770).

Moreover, the vertical heading of Figure S4 should be "RGM conc. (pg m^{-3})" rather than "Hg$^P_{2.5}$ conc. (pg m^{-3})", and we have corrected it (see at line 64).

(8) Lines 276, 278, 281, 282: I suspect the supplemental figure numbers were wrong. Shouldn't they be Figures S1 and S2?

Response:

Thanks for the reviewer's carefully check on these sentences and the Figures S1 and S2. We feel very sorry that we forgot to put Figure S1 (the picture of insulated box) in the supplement. Figure S1 has been added in the revised supplement (see at lines 58-59) of this paper. Therefore, the supplemental figure numbers were wrong in the original supplement, while the supplemental figure numbers were right in the original manuscript. We have made some modifications to ensure that the figure numbers in revised manuscript were consistent with those in revised supplement.

See the revised manuscript at lines 150, 256 258, 261-262, 273 and revised supplement at lines 58, 60, 62, 64.

(9) Lines 330: I don't see bimodal here. There was a third peak below 0.4 μm.

Response:

Thanks for the reviewer's carefully check on the Fig. 5. We fully agree with your comments, and we have corrected the statements in the revised manuscript.

See the revised manuscript at lines 23-24, 307-310, 468.

(10) Lines 367-368: This statement needs support of evidence. I don't see where this came from.

Response:

We do agree with your comment that this inference lacks sufficient evidence. Therefore, this sentence (and the evasion of DGM in local or regional surface seawater of the SCS and surrounding oceans was probably an important source for the GEM in the marine atmosphere.) has been deleted after careful consideration

(11) Line 429: The GEM-Hgp correlation may also indicate the two had oceanic sources in addition to anthropogenic sources.

Response:

Thanks for the in-depth comment. The sentence has been revised as "On the one hand, GEM and Hg^P probably originated from the same sources (including but not limited to anthropogenic and oceanic sources) especially in the PRE and nearshore areas." in the revised manuscript.

See the revised manuscript at lines 406-408.

Response to Reviewer #2's Comments

Anonymous Referee #2:

The manuscript presents ship-based measurements of atmospheric mercury species and dissolved gaseous mercury in the Pearl River Estuary and the South China Sea. The authors used the measurements to infer the sources and sinks of elemental and reactive mercury in the atmosphere, to estimate the sea to air flux of mercury, and to assess how the mercury concentrations in the South China Sea differ from other areas. The manuscript is well-written, and presents the results in clearly with appropriate tables and figures. The authors provide a detailed description of their measurement methods, analyze their observations systematically, and provide support for their main conclusions.

I do not have any major concerns about the manuscript, but a few minor comments as follows:

We are grateful for the precise, valuable and positive comments. We have made corresponding changes in the revised manuscript as highlighted in red color. Please see the responses to the specific comments below. The reviewer's comments are in black and our replies are in blue.

(1) Line 43: Here and elsewhere, I would reword "suffered less influence of human activities" to something like "less influence of fresh emissions."

Response:

Thanks for your suggestion. We have changed the term "human activities" as "fresh emissions" throughout the manuscript.

See the revised manuscript at lines 15, 344.

(2) Line 164: The back trajectories were initiated at 500m much higher than the measurement altitude. This needs justification.

Response:

Thanks for your comment. The arrival heights of back trajectories were set at 500 m to represent the approximate height of the mixing marine boundary layer where atmospheric pollutants were well mixed. We have added "the start height was set at 500 m above sea level to represent the approximate height of the mixing marine boundary layer where atmospheric pollutants were well mixed" in the revised manuscript.

See the revised manuscript at lines 141-142.

(3) Line 172: Fig. S1 does not show the sampling unit.

Response:

Thanks for your carefully check on this sentence and Figure S1. The picture of the sampling unit (Figure S1) has been added in the revised supplement of this paper.

See the revised supplement at line 58.

(4) Line 200: How were non-detects in the RGM and HgP measurements treated?

Response:

Thanks for your comment. This sentence has been revised as "It should be noted that all the observed RGM and Hg^P values were higher than the corresponding blank values, and the average blank values for RGM and Hg^P were subtracted from the samples."

See the revised manuscript at lines 179-181.

(5) Line 331: The bimodal distribution seems less obvious in Fig. 5b.

Response:

We agree with the reviewer that the bimodal distribution seems less obvious in Fig. 5b. As a matter of fact, there were three peaks (< 0.4 μm, 0.7-1.1 μm, 5.8-9.0 μm) although the three-modal distribution was not distinct in Fig. 5. We have corrected the statements in the revised manuscript.

See the revised manuscript at lines 23-24, 307-310, 468.

(6) Line 351-353: I am not convinced that these 1-month observations can be extrapolated to an annual dry deposition flux. I recommend removing that calculation unless there is other evidence supporting its validity.

Response:

Thanks for your comment. Since the South China Sea (SCS) is a tropical sea (4 °N-21 °N), so we can assume that there is no large variation in the average PAR and air temperature etc. over the SCS during the four seasons. Moreover, since our sampling time spans September 2015, so the average RGM and Hg^P values obtained in this sampling period can be roughly considered as the annual mean values. Additionally, Fu et al. (2010) had used the observations (August 2010) in the northern SCS to estimate the annual emission flux of Hg^0 over the SCS. Therefore, we think we can use the data obtained in this study to roughly estimate the dry deposition fluxes of RGM and Hg^P in the SCS.

Reference:

Fu, X., Feng, X., Zhang, G., Xu, W., Li, X., Yao, H., Liang, P., Li, J., Sommar, J., Yin, R., and Liu, N.: Mercury in the marine boundary layer and seawater of the South China Sea: Concentrations, sea/air flux, and implication for land outflow, J. Geophys. Res., 115, D06303, https://doi.org/10.1029/2009JD012958, 2010.

(7) Line 365-367: It is not obvious why the small variability in the Hg0 concentrations implies that the evasion of DGM was an important source of Hg0.

Response:

We do agree with your comment that the small variability in Hg^0 concentrations could not imply that the evasion of DGM was an important source of Hg^0. Therefore, we later realized that this inference lacked sufficient evidence. Therefore, we have deleted this sentence (i.e., and the evasion of DGM in local or regional surface seawater of the SCS and surrounding oceans was probably an important source for the GEM in the marine atmosphere.)

(8) Line 381: It is not clear why are higher RH and lower temperature conducive to Hg2 removal? By gas-particle partitioning?

Response:

Thanks for your comment. Yes, by gas-particle partitioning. Previous studies demonstrated that higher RH and lower air temperature were conductive to the transfer of RGM to Hg^P (Rutter and Schauer, 2007; Lee et al., 2016). Thus, we revised the description as "the transfer of RGM to Hg^P due to higher RH and lower air temperature in nighttime (Rutter and Schauer, 2007; Lee et al., 2016)." in the revised manuscript.

See the revised manuscript at lines 357-359.

Reference:

Rutter, A. P., and Schauer, J. J.: The effect of temperature on the gas–particle partitioning of reactive mercury in atmospheric aerosols, Atmos. Environ., 41, 8647–8657, https://doi.org/10.1016/j.atmosenv.2007.07.024, 2007.

Lee, G.-S., Kim, P.-R., Han, Y.-J., Holsen, T. M., Seo, Y.-S., and Yi, S.-M.: Atmospheric speciated mercury concentrations on an island between China and Korea: sources and transport pathways, Atmos. Chem. Phys., 16, 4119-4133, https://doi.org/10.5194/acp-16-4119-2016, 2016.

(9) Please mention in the main text that the acronyms are defined in the appendix.

Response:

Thanks for your suggestion. The sentence "It should be noted that all of the acronyms in this article have been listed in the Appendix." has been added in the revised manuscript.

See the revised manuscript at lines 45-46.

(10) Fig. 5: Using the same scales for the y-axes on panels a and b will be helpful.

Response:

Thanks for the suggestion. We have set the same scales for the Y-axes on panels a and b in Fig.5.

See the revised manuscript at line 776.

(11) Fig. 6: The PAR values can be removed. They do not add much information, but clutter the figure.

Response:

Thanks for your suggestion. There are no PAR values in Fig. 6, and I suspect that the PAR values you mentioned are the one in Fig. 7. First of all, the PAR data was essential for the following discussions. Moreover, we have changed the filled color for the RGM concentrations in nighttime. Thus, we feel the revised Fig. 7 is clearer now.

See the revised manuscript at line 782.

(12) Fig. 9: How are the point measurements interpolated for the entire region? Was this interpolation necessary to calculate the sea-air flux? If not may be show the measurements like those in Fig. 3b.

Response:

Thanks for your comments and suggestions. The Fig. 9 was plotted by the software of Ocean Data View based on the data obtained at each the sampling station. It is not necessary for the interpolation to calculate the sea-air flux of Hg^0. The DGM concentrations in surface seawater and emission fluxes of Hg^0 at all stations have been symbolized in the revised Fig. 9 like those in Fig. 3b.

See the revised manuscript at line 789.

(13) Table 2: The correlation coefficients for HgP(2.5)-RGM and RGM-HgP(2.5) differ. Is that correct?

Response:

We feel very sorry for our carelessness. After recalculation, the correlation coefficients for $Hg^P_{2.5}$-RGM and RGM-$Hg^P_{2.5}$ were same ($p < 0.01$, $r = 0.453$). We have corrected the p and r values for $Hg^P_{2.5}$-RGM in Table 2.

See the revised manuscript at lines 794-795.

Speciated atmospheric mercury and sea-air exchange of gaseous mercury in the South China Sea

Chunjie Wang[1], Zhangwei Wang[1], Fan Hui[2], Xiaoshan Zhang[1]

[1] Research Center for Eco-Environmental Sciences, Chinese Academy of Sciences, 18 Shuangqing Road, Beijing, China

[2] China University of Petroleum (Beijing), 18 Fuxue Road, Beijing, China

Correspondence to: Xiaoshan Zhang (zhangxsh@rcees.ac.cn)

Abstract

The characteristics of the reactive gaseous mercury (RGM) and particulate mercury (Hg^P) in the marine boundary layer (MBL) is poorly understood due in part to sparse data from sea and ocean. Gaseous elemental Hg (GEM), RGM and size-fractioned Hg^P in marine atmosphere, and dissolved gaseous Hg (DGM) in surface seawater were determined in the South China Sea (SCS) during an oceanographic expedition (3–28 September 2015). The mean concentrations of GEM, RGM and $Hg^P_{2.5}$ were 1.52 ± 0.32 ng m^{-3}, 6.1 ± 5.8 pg m^{-3} and 3.2 ± 1.8 pg m^{-3}, respectively. Low GEM level indicated that the SCS suffered less influence from fresh emissions, which could be due to the majority of air masses coming from the open oceans as modeled by backward trajectories. Atmospheric reactive Hg (RGM + $Hg^P_{2.5}$) represented less than 1 % of total atmospheric Hg, indicating that atmospheric Hg existed mainly as GEM in the MBL. The GEM and RGM concentrations (1.73 ± 0.40 ng m^{-3} and 7.1 ± 1.4 pg m^{-3} respectively) in the northern SCS were significantly higher than those (1.41 ± 0.26 ng m^{-3} and 3.8 ± 0.7 pg m^{-3}) in the western SCS, and the $Hg^P_{2.5}$ and Hg^P_{10} levels (8.3 and 24.4 pg m^{-3}) in the Pearl River Estuary (PRE) were 0.5–6.0 times higher than those in the open waters of the SCS, indicating that the PRE was polluted to some extent. The size distribution of Hg^P in PM_{10} was observed to be three-modal with peaks around <0.4 μm, 0.7–1.1 μm and 5.8–9.0 μm, respectively, but the coarse modal was the dominant size, especially in the open SCS. There was no significant diurnal variation of GEM and $Hg^P_{2.5}$, but we found the RGM concentrations were significantly higher in daytime (8.0 ± 5.5 pg m^{-3}) than in nighttime (2.2 ± 2.7 pg m^{-3}) mainly due to the influence of solar radiation. In the northern SCS, the DGM concentrations in nearshore area (40−55 pg l^{-1}) were about twice as high as those in the open sea, but this pattern was not significant in the western SCS. The sea-air exchange fluxes of Hg^0 in the SCS varied from 0.40 to 12.71 ng m^{-2} h^{-1} with a mean value of 4.99 ± 3.32 ng m^{-2} h^{-1}. The annual emission flux of Hg^0 from the SCS to the atmosphere was estimated to be 159.6 tons yr^{-1}, accounting for about 5.54 % of the global Hg^0 oceanic evasion though the SCS only represents 1.0 % of the global ocean area. Additionally, the annual dry deposition flux of atmospheric reactive Hg represented more than 18 % of the annual evasion flux of Hg^0, and

35   therefore the dry deposition of atmospheric reactive Hg was an important pathway for the input of

36   atmospheric Hg to the SCS.

1   Introduction

38   Mercury (Hg) is a naturally occurring metal. Hg is released to the environment through both the

39   natural and anthropogenic pathways (Schroeder and Munthe, 1998). However, since the Industrial

40   Revolution, the anthropogenic emissions of Hg increased drastically. Continued rapid

41   industrialization has made Asia the largest source region of Hg emissions to air, with East and

42   Southeast Asia accounting for about 40 % of the global total (UNEP, 2013). Three operationally

43   defined Hg forms are present in the atmosphere: gaseous elemental Hg (GEM or Hg^0), reactive

44   gaseous Hg (RGM) and particulate Hg (Hg^P) (Schroeder and Munthe, 1998; Landis et al., 2002),

45   while they have different physicochemical characteristics. It should be noted that all of the

46   acronyms in this article have been listed in the Appendix. GEM is very stable with a residence

47   time of 0.2−1.0 yr due to its high volatility and low solubility (Radke et al., 2007; Selin et al.,

48   2007; Horowitz et al., 2017). Therefore, GEM can be transported for a long-range distance in the

49   atmosphere, and this makes it well-mixed on a regional and global scale. Generally, GEM makes

50   up more than 95 % of total atmospheric Hg (TAM), while the RGM and Hg^P concentrations

51   (collectively known as atmospheric reactive mercury) are typically 2−3 orders of magnitude

52   smaller than GEM in part because they are easily removed from ambient air by wet and dry

53   deposition (Laurier and Mason, 2007; Holmes et al., 2009; Gustin et al., 2013), and they can also

54   be reduced back to Hg^0.

55   Numerous previous studies have shown that Hg^0 in the marine boundary layer (MBL) can be

56   rapidly oxidized to form RGM in situ (Laurier et al., 2003; Sprovieri et al., 2003, 2010; Laurier

57   and Mason, 2007; Soerensen et al., 2010a; Wang et al., 2015; Mao et al., 2016; Ye et al., 2016).

58   Ozone and OH could potentially be important oxidants on aerosols (Ariya et al., 2015; Ye et al.,

59   2016), while the reactive halogen species (e.g., Br, Cl and BrO, generating from sea salt aerosols)

60   may be the dominant sources for the oxidation of Hg^0 in the MBL (Holmes et al., 2006, 2010;

61   Auzmendi-Murua et al., 2014; Gratz et al., 2015; Steffen et al., 2015; Shah et al., 2016; Horowitz

62   et al., 2017). However, a recent study showed that Br and BrO became dominant GEM oxidants in

63   the marine atmosphere with mixing ratios reaching 0.1 and 1 pptv, respectively, and contributing ~

64   70 % of the total RGM production during midday, while O_3 dominated GEM oxidation (50–90 %

65   of RGM production) when Br and BrO mixing ratios were diminished (Ye et al., 2016). The wet

66   and dry deposition (direct or uptake by sea-salt aerosol) represents a major input of RGM and Hg^P

67   to the sea and ocean due to their special and unique characteristics (i.e., high reactivity and water

68   solubility) (Landis et al., 2002; Holmes et al., 2009). Previous studies also showed that

69   atmospheric wet and dry deposition of RGM (mainly $HgBr_2$, $HgCl_2$, HgO, Hg-nitrogen and sulfur

70   compounds) was the greatest source of Hg to open oceans (Holmes et al., 2009; Mason et al., 2012;

2

71 Huang et al., 2017). A recent study suggested that approximately 80 % of atmospheric reactive Hg
72 sinks into the global oceans, and most of the deposition takes place to the tropical oceans
73 (Horowitz et al., 2017).

74 The atmospheric reactive Hg deposited to the oceans follows different reaction pathways.
75 One important process is that divalent Hg can be combined with the existing particles followed by
76 sedimentation, or be converted to methylmercury (MeHg), the most bioaccumulative and toxic
77 form of Hg in seafood (Ahn et al., 2010; Mason et al., 2017). Another important process is that the
78 divalent Hg can be converted to dissolved gaseous Hg (DGM) through abiotic and biotic
79 mechanisms (Strode et al., 2007). It is well known that almost all DGM in the surface seawater is
80 Hg^0 (Horvat et al., 2003), while the dimethylmercury is extremely rare in the surface seawater
81 (Bowman et al., 2015). It has been found that a majority of the surface seawater was
82 supersaturated with respect to Hg^0 (Soerensen et al., 2010b, 2013, 2014), and parts of this Hg^0
83 may be emitted to the atmosphere. Evasion of Hg^0 from the oceanic surface into the atmosphere is
84 partly driven by the solar radiation and aquatic Hg pools of natural and anthropogenic origins
85 (Andersson, et al., 2011). Sea-air exchange is an important component of the global Hg cycle as it
86 mediates the rate of increase in ocean Hg and therefore the rate of change in level of MeHg.
87 Consequently, Hg^0 evasion from sea surface not only decreases the amount of Hg available for
88 methylation in waters but also has an important effect on the redistribution of Hg in the global
89 environment (Strode et al., 2007).

90 In recent years, speciated atmospheric Hg has been monitored in coastal areas (Xu et al.,
91 2015; Ye et al., 2016; Howard et al., 2017; Mao et al., 2017) and open seas and oceans (e.g.,
92 Chand et al., 2008; Soerensen et al., 2010a; Mao et al., 2016; Wang et al., 2016a, b). However,
93 there exists a dearth of knowledge regarding speciated atmospheric Hg and sea-air exchange of
94 Hg^0 in tropical seas, such as the South China Sea (SCS). The highly time-resolved ambient GEM
95 concentrations were measured using a Tekran[®] system. Simultaneously, the RGM, Hg^P and DGM
96 were measured using manual methods. The main objectives of this study are to identify the
97 spatial-temporal characteristics of speciated atmospheric Hg and to investigate the DGM
98 concentrations in the SCS during the cruise, and then to calculate the Hg^0 flux based on the
99 meteorological parameters as well as the concentrations of GEM in air and DGM in surface
100 seawater. These results will raise our knowledge of the Hg cycle in tropical marine atmosphere
101 and waters.

102 **2   Materials and methods**

103 **2.1   Study area**

104 The SCS is located in the downwind of Southeast Asia (Fig. 1a), and it is the largest semi-enclosed
105 marginal sea in the western tropical Pacific Ocean. The SCS is connected with the East China Sea
106 (ECS) to the northeast and the western Pacific Ocean to the east (Fig. 1a). The SCS is surrounded

by numerous developing and developed countries (Fig. 1a). An open cruise was organized by the South China Sea Institute of Oceanology (Chinese Academy of Sciences) and conducted during the period of 3−28 September 2015. The sampling campaign was conducted on R/V *Shiyan 3*, which departed from Guangzhou, circumnavigated the northern and western SCS and then returned to Guangzhou. The DGM sampling stations and R/V tracks are plotted in Fig. 1b. In this study, meteorological parameters (including photosynthetically available radiation (PAR) (Li-COR®, Model: Li-250), wind speed, air temperature and RH) were measured synchronously with atmospheric Hg onboard the R/V.

2.2 Experimental methods

2.2.1 Atmospheric GEM measurements

In this study, GEM was measured using an automatic dual channel, single amalgamation cold vapor atomic fluorescence analyzer (Model 2537B, Tekran®, Inc., Toronto, Canada), which has been reported in our previous studies (Wang et al., 2016a, b, c). In order to reduce the contamination from ship exhaust plume as possible, we installed the Tekran® system inside the ship laboratory (the internal air temperature was controlled to 25 ℃ using an air conditioner) on the fifth deck of the R/V and mounted the sampling inlet at the front deck 1.5 m above the top deck (about 16 m above sea level) using a 7 m heated (maintained at 50 ℃) polytetrafluoroethylene (PTFE) tube (¼ inch in outer diameter). The sampling interval was 5 min and the air flow rate was 1.5 l min^{-1} in this study. Moreover, two PTFE filters (0.2 μm pore size, 47 mm diameter) were positioned before and after the heated line, and the soda lime before the instrument was changed every 3 days during the cruise. The Tekran® instrument was calibrated every 25 h using the internal calibration source and these calibrations were checked by injections of certain volume of saturated Hg^0 before and after this cruise. The relative percent difference between manual injections and automated calibrations was < 5 %. The precision of the analyzer was determined to > 97 %, and the detection limit was < 0.1 ng m^{-3}.

The meteorological and basic seawater parameters were collected onboard the R/V, which was equipped with meteorological and oceanographic instrumentations. To investigate the influence of air masses movements on the GEM levels, 72-h backward trajectories of air masses were calculated using the Hybrid Single Particle Lagrangian Integrated Trajectory (HYSPLIT) model (Draxler and Rolph, 2012) and TrajStat software (Wang et al., 2009) based on Geographic Information System. Global Data Assimilation System (GDAS) meteorological dataset (ftp://arlftp.arlhq.noaa.gov/pub/archives/gdas1/) with $1\degree \times 1\degree$ latitude and longitude horizontal spatial resolution and 23 vertical levels at 6-h intervals was used as the HYSPLIT model input. It should be noted that the start time of each back trajectory was identical to the GEM sampling time (UTC) and the start height was set at 500 m above sea level to represent the approximate height of the mixing marine boundary layer where atmospheric pollutants were well mixed.

2.2.2 Sampling and analysis of RGM and Hg^P

The $Hg^P_{2.5}$ (Hg^P in $PM_{2.5}$) was collected on quartz filter (47 mm in diameter, Whatman), which has been reported in several previous studies (Landis et al., 2002; Liu et al., 2011; Kim et al., 2012;). It should be pointed out that the KCl coated denuders were heated at 500 ℃ for 1 h and the quartz filters were pre-cleaned by pyrolysis at 900 ℃ for 3 h to remove the possible pollutant. The RGM and $Hg^P_{2.5}$ were sampled using a manual system (URG-3000M), which has been reported in previous studies (Landis et al., 2002; Liu et al., 2011; Wang et al., 2016b). The sampling unit includes an insulated box (Fig. S1), two quartz annular denuders, two Teflon filter holder (URG Corporation) and a pump etc. The sampling flow rate was $10\,l\,min^{-1}$ (Landis et al., 2002), and the sampling inlet was 1.2 m above the top deck of the R/V. In this study, one $Hg^P_{2.5}$ sample was collected in the daytime (6:00–18:00) and the other in the nighttime (18:00–6:00 (next day)), while two RGM samples were collected in the daytime (6:00–12:00 and 12:00–18:00, local time) and one RGM sample in the nighttime. Quality assurance and quality control for Hg^P and RGM were carried out using field blank samples and duplicates. The field blank denuders and quartz filters were treated similarly to the other samples but not sampling. The mean relative differences of duplicated $Hg^P_{2.5}$ and RGM samples (n = 6) were 13 $\pm$6 % and 9 $\pm$7 %, respectively.

Meanwhile, we collected different size particles using an Andersen impactor (nine-stage), which has been widely used in previous studies (Feddersen et al., 2012; Kim et al., 2012; Zhu et al., 2014; Wang et al., 2016a). The Andersen cascade impactor was installed on the front top deck of the R/V to sample the size-fractioned particles in PM_{10}. In order to diminish the contamination from exhaust plume of the ship as much as possible, we turned off the pump when R/V arrived at stations, and then switched back on when the R/V went to next station. The sample collection began in the morning (10:00 am) and continued for 2 days with a sampling flow rate of 28.3 l min^{-1}. Field blanks for Hg^P were collected by placing nine pre-cleaned quartz filters (81 mm in diameter, Whatman) in another impactor for 2 days without turning on the pump. After sampling, the quartz filters were placed in cleaned plastic boxes (sealing in Zip Lock plastic bags), and then were immediately preserved at −20 ℃ until the analysis.

The detailed analysis processes of RGM and Hg^P have been reported in our previous studies (Wang et al., 2016a, b). Briefly, the denuder and quartz filter were thermally desorbed at 500 ℃ and 900 ℃, respectively, and then the resulting thermally decomposed Hg^0 in carrier gas (zero air, i.e., Hg-free air) was quantified. The method detection limit was calculated to be 0.67 pg m^{-3} for RGM based on 3 times the standard deviation of the blanks (n = 57) for the whole dataset. The average field blank of denuders was 1.2 $\pm$0.6 pg (n = 6). The average blank values (n = 6) of $Hg^P_{2.5}$ and Hg^P_{10} were 1.4 pg (equivalent of < 0.2 pg m^{-3} for a 12 h sampling time) and 3.2 pg (equivalent of < 0.04 pg m^{-3} for a 2-day sampling time) of Hg per filter, respectively. The detection limits of $Hg^P_{2.5}$ and Hg^P_{10} were all less than 1.5 pg m^{-3} based on 3 times the standard deviation of field blanks. It should be noted that all the observed RGM and Hg^P values were

2.2.3 Determination of DGM in surface seawater

In this study, the analysis was carried out according to the trace element clean technique, all containers (borosilicate glass bottles and PTFE tubes, joints and valves) were cleaned prior to use with detergent, followed by trace-metal-grade HNO$_3$ and HCl, and then rinsed with Milli-Q water (> 18.2 MΩ cm^{-1}), which has been described in our previous study (Wang et al., 2016c). DGM were measured in situ using a manual method (Fu et al., 2010; Ci et al., 2011). The detailed sampling and analysis of DGM has been elaborated in our previous study (Wang et al., 2016c). The analytical blanks were conducted onboard the R/V by extracting Milli-Q water for DGM. The mean concentration of DGM blank was 2.3 ± 1.2 pg l^{-1} (n = 6), accounting for 3−10 % of the raw DGM in seawater samples. The method detection limit was 3.6 pg l^{-1} on the basis of three times the standard deviation of system blanks. The relative standard deviation of duplicate samples generally < 8 % of the mean concentration (n = 6).

2.2.4 Estimation of sea-air exchange flux of Hg^0

The sea-air flux of Hg^0 was calculated using a thin film gas exchange model developed by Liss and Slater (1974) and Wanninkhof (1992). The detailed calculation processes of Hg^0 flux have been reported in recent studies (Ci et al., 2011; Kuss, 2014; Wang et al., 2016c; Kuss et al., 2018). It should be noted that the Schmidt number for gaseous Hg (Sc_{Hg}) is defined as the following equation: $Sc_{Hg} = v/D_{Hg}$, where v is the kinematic viscosity (cm^2 s^{-1}) of seawater calculated using the method of Wanninkhof (1992), D_{Hg} is the Hg^0 diffusion coefficient (cm^2 s^{-1}) in seawater, which is calculated according to the recent research (Kuss, 2014). The degree of Hg^0 saturation (S_a) was calculated using the following equation: $S_a = H' DGM_{conc}/GEM_{conc}$, and the calculation of H' (the dimensionless Henry's Law constant) has been reported in previous studies (Ci et al., 2011, 2015; Kuss, 2014).

3 Results and discussion

3.1 Speciated atmospheric Hg concentrations

Figure 2 shows the time series of speciated atmospheric Hg and meteorological parameters during the cruise in the SCS. The GEM concentration during the whole study period ranged from 0.92 to 4.12 ng m^{-3} with a mean value of 1.52 ± 0.32 ng m^{-3} (n = 4673), which was comparable to the average GEM levels over the global oceans (1.4−1.6 ng m^{-3}, Soerensen et al., 2010a, 2013) and Atlantic Ocean (1.52 ± 0.32 ng m^{-3}, Laurier and Mason, 2007), and higher than those at background sites in the Southern Hemisphere (0.85−1.05 ng m^{-3}, Slemr et al., 2015; Howard et al., 2017), and also higher than those in remote oceans, such as the Cape Verde Observatory

214   station (1.19 ± 0.13 ng m^{-3}, Read et al., 2017), equatorial Pacific Ocean ($1.15-1.05$ ng m^{-3},

215   Soerensen et al., 2014) and Indian Ocean ($1.0-1.2$ ng m^{-3}, Witt et al., 2010; Angot et al., 2014),

216   but lower than those in marginal seas, such as the Bohai Sea (BS), Yellow Sea (YS) and East

217   China Sea (ECS) (Table 1). However, previous studies conducted in the northern SCS showed that

218   the average GEM concentrations in their study period ($2.6-3.5$ ng m^{-3}, Fu et al., 2010; Tseng et al.,

219   2012) were higher than that in this study. This is due to the fact that the GEM level in the northern

220   SCS (Fu et al., 2010; Tseng et al., 2012) were considerably higher than that in the western SCS

221   (this study).

222   The Hg$^P_{2.5}$ concentrations over the SCS ranged from 1.2 to 8.3 pg m^{-3} with a mean value of

223   3.2 ± 1.8 pg m^{-3} (n = 39) (Fig. 2), which was higher than those observed at Nam Co (China) and

224   the Amsterdam Island, and were comparable to those in other coastal areas, such as the Okinawa

225   Island, the Nova Scotia, the Adriatic Sea, the Ontario lake and the Weeks Bay (see Table 1), but

226   lower than those in the BS and YS (Wang et al., 2016b), and considerably lower than those in

227   rural and urban sites, such as Xiamen, Seoul (see Table 1), Guiyang and Waliguan (Fu et al., 2011,

228   2012). The results showed that the SCS suffered less influence from human activities. The RGM

229   concentration over the SCS ranged from 0.27 to 27.57 pg m^{-3} with a mean value of 6.1 ± 5.8 pg

230   m^{-3} (n = 58), which was comparable to those in other seas, such as the North Pacific Ocean, the

231   North Atlantic Ocean and the Mediterranean Sea (including the Adriatic Sea) (Table 1), and higher

232   than the global mean RGM concentration in the MBL (Soerensen et al., 2010a), and also higher

233   than those measured at a few rural sites (Valente et al., 2007; Liu et al., 2010; Cheng et al., 2013,

234   2014), but significantly much lower than those polluted urban areas in China and South Korea,

235   such as Guiyang (35.7 ± 43.9 pg m^{-3}, Fu et al., 2011), Xiamen, and Seoul (Table 1). Furthermore,

236   Figure 2 shows that the long-lived GEM has smaller variability compared to the short-lived

237   species like RGM and Hg$^P_{2.5}$, indicating that atmospheric reactive Hg was easily scavenged from

238   the marine atmosphere due not only to their characteristics (high activity and solubility) but also

239   due to their sensitivity to meteorological conditions and chemical environments. This pattern was

240   consistent with our previous observed patterns in the BS and YS (Wang et al., 2016b). Moreover,

241   we found that atmospheric reactive Hg represents less than 1 % of TAM in the atmosphere, which

242   was comparable to those measured in other marginal and inner seas, such as the BS and YS (Wang

243   et al., 2016b), Adriatic Sea (Sprovieri and Pirrone, 2008), Okinawa Island (located in the ECS)

244   (Chand et al., 2008), but was significantly lower than those at the urban sites (Table 1).

3.2   Spatial distribution of atmospheric Hg

3.2.1   Spatial distributions of GEM and RGM

247   The spatial distribution of GEM over the SCS is illustrated in Fig. 3a. The mean GEM

248   concentration in the northern SCS (1.73 ± 0.40 ng m^{-3} with a range of $1.01-4.12$ ng m^{-3}) was

249   significantly higher than that in the western SCS (1.41 ± 0.26 ng m^{-3} with a range of $0.92-2.83$ ng

250 m^{-3}) (*t*-test, $p < 0.01$). Additionally, we found that the GEM concentrations in the PRE (the

251 average value > 2.00 ng m^{-3}) were significantly higher than those in the open SCS (see Figs. 2, 3a),

252 indicating that this nearshore area suffered from high GEM pollution in our study period probably

253 due to the surrounding human activities. Figure 3a shows that there was large difference in GEM

254 concentration between stations 1−10 and stations 16−31. The 72-h back-trajectories of air masses

255 showed that the air masses with low GEM levels between stations 1 and 10 mainly originated

256 from the SCS (Fig. S2a), while the air masses with high GEM levels at stations 16−31 primarily

257 originated from East China and ECS, and then passed over the southeast coastal regions of China

258 (Fig. S2b). Additionally, Fig. 3a shows that there was small variability of GEM concentrations

259 over the western SCS except the measurements near the station 79. The back-trajectories showed

260 that the air masses with elevated GEM level near the station 79 originated from the south of the

261 Taiwan Island, while the other air masses mainly originated from the West Pacific Ocean (Fig. S3a)

262 and the Andaman Sea (Fig. S3b). Therefore, the air masses dominantly originated from sea and

263 ocean in this study period, and this could be the main reason for the low GEM level over the SCS.

264 In conclusion, GEM concentrations showed a conspicuous dependence on the sources and

265 movement patterns of air masses during this cruise.

266 The spatial distribution of RGM over the SCS is plotted in Fig. 3b. The mean RGM

267 concentration in the northern SCS (7.1 ± 1.4 pg m^{-3}) was also obviously higher than that in the

268 western SCS (3.8 ± 0.7 pg m^{-3}) (*t*-test, $p < 0.05$), indicating that a portion of RGM in the northern

269 SCS maybe originated from the anthropogenic emission. We observed elevated RGM

270 concentrations in the PRE, and which was consistent with the GEM distribution pattern, indicating

271 that part of the RGM near PRE probably originated from the surrounding human activities. This is

272 confirmed by the following fact: The RGM concentrations in nighttime of the two days in the PRE

273 were 11.3 and 5.2 pg m^{-3} (Figs. 3b and S4), and they were significantly higher than those in the

274 open SCS. Another obvious feature is that the amplitude of RGM concentration is much greater

275 than the GEM, and this further indicated that the RGM was easily removed from the atmosphere

276 through both the wet and dry deposition. In addition, we found that the RGM concentrations in the

277 nearshore area were not always higher than those in the open sea except the measurements in the

278 PRE, suggesting that the RGM in the remote marine atmosphere presumably not originated from

279 land but from the in situ photo-oxidation of Hg^0, which had been reported in previous studies (e.g.,

280 Hedgecock and Pirrone, 2001; Lindberg et al., 2002; Laurier et al., 2003; Sprovieri et al., 2003,

281 2010; Sheu and Mason, 2004; Laurier and Mason, 2007; Soerensen et al., 2010a; Wang et al.,

282 2015).

283 ### 3.2.2 Spatial distributions of Hg$^P_{2.5}$ and Hg$^P_{10}$

284 The concentrations and spatial distribution of Hg$^P_{2.5}$ in the MBL are illustrated in Fig. 4a. The

285 highest Hg$^P_{2.5}$ value (8.3 pg m^{-3}) was observed in the PRE during daytime on 4 September 2015

286 presumably due to the local human activities. The homogeneous distribution and lower level of

287 $Hg^P_{2.5}$ in the open SCS indicated that the $Hg^P_{2.5}$ not originated from the land and the SCS suffered

288 less influence from human activities especially in the open sea. This is due to the fact that the

289 majority of air masses in the SCS during this study period came from the seas and oceans. The

290 spatial distribution pattern of $Hg^P_{2.5}$ in this study was different from our previous observed

291 patterns in the BS and YS (Wang et al., 2016b), which showed that $Hg^P_{2.5}$ concentrations in

292 nearshore area were higher than those in the open sea both in spring and fall mainly due to the

293 outflow of atmospheric Hg^P from East China.

294   The concentrations and spatial distributions of Hg^P_{10} in the MBL of the SCS are illustrated in

295 Fig. 4b. We found that the Hg^P_{10} concentration was considerably (1–6 times) higher in the PRE

296 than those of other regions of the SCS probably due to the large emissions of anthropogenic Hg in

297 surrounding areas of the PRE. Moreover, the highest $Hg^P_{2.1}/Hg^P_{10}$ ratio (41 %) was observed in the

298 PRE and coastal sea area of Hainan Island, while lowest ratio (22 %) was observed in the open sea

299 (Fig. 4b). The Hg^P_{10} concentrations and $Hg^P_{2.1}/Hg^P_{10}$ ratios were higher in the nearshore area

300 compared to those in the open sea, demonstrating that coastal sea areas are polluted by

301 anthropogenic Hg to a certain extent. Interestingly, we found the mean $Hg^P_{2.1}$ concentration (3.16

302 $\pm$ 2.69 pg m^{-3}, n = 10) measured using the Andersen sampler was comparable to the mean $Hg^P_{2.5}$

303 concentration (3.33 $\pm$ 1.89 pg m^{-3}, n = 39) measured using a 47 mm Teflon filter holder (t-test, p >

304 0.1). This indicated that the fine Hg^P level in the MBL of the SCS was indeed low, and there might

305 be no significant difference in Hg^P concentration in the SCS between 12 h and 48 h sampling time.

306   The concentrations of all size-fractioned Hg^P are summarized in Table S1. The size

307 distribution of Hg^P in the MBL of the SCS is plotted in Fig. 5. One striking feature is that the

308 three-modal pattern with peaks around <0.4 μm, 0.7–1.1 μm and 5.8–9.0 μm was observed for the

309 size distributions of Hg^P in the open sea (Fig. 5a) if we excluded the data in the PRE. The

310 three-modal pattern was more obvious when we consider all the data (Fig. 5b). Generally, the Hg^P

311 concentrations in coarse particles were significantly higher than those in fine particles, and $Hg^P_{2.1}$

312 contributed approximately 32 % (22–41 %, see Fig. 4b) to the Hg^P_{10} for the whole data, indicating

313 that the coarse mode was the dominant size during this study period. This might be explained by

314 the sources of the air masses. Since air masses dominantly originated from sea and ocean (Figs. S1,

315 S2) and contained high concentrations of sea salts which generally exist in the coarse mode (1–10

316 μm) (Athanasopoulou et al., 2008; Mamane et al., 2008), the $Hg^P_{2.1}/Hg^P_{10}$ ratios were generally

317 lower in the SCS compared to those in the BS, YS and ECS (Wang et al., 2016a).

3.3   Dry deposition fluxes of RGM and Hg^P

319 The dry deposition flux of Hg^P_{10} was obtained by summing the dry deposition fluxes of each

320 size-fractionated Hg^P in the same set. The dry deposition flux of Hg^P_{10} is calculated using the

321 following equation: $F = \sum CHg^P \times V_d$, the F is the dry deposition flux of Hg^P_{10} (ng m^{-2} d^{-1}), CHg^P

322   is the concentration of Hg^P in each size fraction (pg m^{-3}), and V_d is the corresponding dry

323   deposition velocity (cm s^{-1}). In this study, the dry deposition velocities of 0.03, 0.01, 0.06, 0.15

324   and 0.55 cm s^{-1} (Giorgi, 1988; Pryor et al., 2000; Nho-Kim et al., 2004) were chosen for the

325   following size-fractioned particles: < 0.4, 0.4–1.1, 1.1–2.1, 2.1–5.8 and 5.8–10 μm, respectively

326   (Wang et al., 2016a). The average dry deposition flux of Hg^P_{10} was estimated to be 1.08 ng m^{-2} d^{-1}

327   based on the average concentrations of each size-fractionated Hg^P in the SCS (Table S2), which

328   was lower than those in the BS, YS and ECS (Wang et al., 2016a). The dry deposition velocity of

329   RGM was 4.0–7.6 cm s^{-1} because of its characteristics and rapid uptake by sea salt aerosols

330   followed by deposition (Poissant et al., 2004; Selin et al., 2007). The annual dry deposition fluxes

331   of Hg^P_{10} and RGM to the SCS were calculated to be 1.42 and 27.39–52.05 tons yr^{-1} based on the

332   average Hg^P_{10} and RGM concentrations and the area of the SCS (3.56×10^{12} m^2). The result

333   showed that RGM contributed more than 95 % to the total dry deposition of atmospheric reactive

334   Hg. The annual dry deposition flux of RGM was considerably higher than that of the Hg^P_{10} due to

335   the higher deposition rate and concentrations of RGM.

3.4   Temporal variation of atmospheric Hg

3.4.1   diurnal variation of GEM

338   The diurnal variation of GEM concentration during the whole study period is illustrated in Fig. 6.

339   It was notable that there was no significant variability of the mean ($\pm$ SD) GEM concentration in a

340   whole day during this study period, and the GEM concentration dominantly fell in the range of

341   1.3–1.7 ng m^{-3} (Fig. 6). The statistical result showed that the mean GEM concentration in the

342   daytime (6:00–18:00) (1.49 ± 0.06 pg m^{-3}) was comparable to that in the nighttime (1.51 ± 0.06

343   pg m^{-3}) (t-test, $p > 0.05$). The lower GEM concentrations and smaller variability over the SCS

344   further revealed that the SCS suffered less influence of fresh emissions.

3.4.2   Daily variation of RGM

346   The average RGM concentrations in the daytime and nighttime are illustrated in Fig. 7. Firstly, it

347   could be found that RGM showed a diurnal variation with higher concentrations in the daytime

348   and lower concentrations in the nighttime during the whole study period. The mean RGM

349   concentration in the daytime (8.0 ± 5.5 pg m^{-3}) was significantly and considerably higher than that

350   in the nighttime (2.2 ± 2.7 pg m^{-3}) (t-test, $p < 0.001$). This diurnal pattern was in line with the

351   previous multiple sites studies (Laurier and Mason, 2007; Liu et al., 2007; Engle et al., 2008;

352   Cheng et al., 2014). This is due to the fact that the oxidation of GEM in the MBL must be

353   photochemical, which have been evidenced by the diurnal cycle of RGM (Laurier and Mason,

354   2007). Another reason is that there was more Br (gas phase) production during daytime (Sander et

355   al., 2003). Figure S3 showed that the RGM concentration in the nighttime was lower than those in

356   corresponding forenoon and afternoon except the measurements in the PRE. This further indicated

that (1) the RGM originated from the photo-oxidation of Hg^0 in the atmosphere and (2) the transfer of RGM to Hg^P due to higher RH and lower air temperature in nighttime (Rutter and Schauer, 2007; Lee et al., 2016).

In addition, we found that the difference in RGM concentration between day and night in the SCS was higher than those in the BS and YS (Wang et al., 2016b), and one possible reason is that the solar radiation and air temperature over the SCS were stronger and higher compared to those over the BS and YS (Wang et al., 2016b) as a result of the specific location of the SCS (tropical sea) and the different sampling season (the SCS: September 2015, the BS and YS: April−May and November 2014). Secondly, it could be found that the higher the RGM concentrations in the daytime, and the higher the RGM concentrations in the nighttime, but the concentrations in daytime were higher than that in the corresponding nighttime throughout the sampling period (see Figs. 7, S3). This is partly because the higher RH and lower air temperature in nighttime were conductive to the removal of RGM (Rutter and Schauer, 2007; Amos et al., 2012). Thirdly, we found that the difference in RGM concentration between different days was large though there was no significantly difference in PAR values (Fig. 7). However, here again divide two kinds of cases: the first kind of circumstance is that the higher RGM in the PRE (day and night) presumably mainly originated from the surrounding human activities (i.e., 4−5 September 2015); the second scenario is that RGM in open waters mainly originated from the in situ oxidation of GEM in the MBL (Soerensen et al., 2010a; Sprovieri et al., 2010). The main reason for the large difference in RGM concentration between different days was that there was large difference in wind speed and RH between different days (see Fig. 2), and the discussion can be found in the following paragraphs.

3.4.3 Daily variation of $Hg^P_{2.5}$

Figure 8 shows the $Hg^P_{2.5}$ concentrations in the daytime and nighttime during the entire study period. The $Hg^P_{2.5}$ value in the daytime (3.4 ± 1.9 pg m^{-3}, n = 20) was slightly but not significantly higher than that in the nighttime (2.4 ± 0.9 pg m^{-3}, n = 19) (t-test, $p > 0.1$), and this pattern was consistent with the result of our previous study conducted in the open waters of YS (Wang et al., 2016b). The elevated $Hg^P_{2.5}$ concentrations in the PRE and nearshore area of the Hainan Island (Fig. 4 and Fig. 8) indicated that the nearshore areas were readily polluted due to the anthropogenic Hg emissions, while the low $Hg^P_{2.5}$ level in the open sea further suggested that the open areas of the SCS suffered less anthropogenic Hg^P. Therefore, we postulate that the $Hg^P_{2.5}$ over the open SCS mainly originated from the in situ formation.

During the cruise in the western SCS (16−28 September 2015), we found elevated $Hg^P_{2.5}$ concentrations when the RGM concentrations were high at lower wind speed (e.g., 20−22 September 2015, it was sunny all these days) (see Figs. 2, 7, 8). This is probably due to the transferring of RGM from the gas to the particle phase. In contrast, we found that the $Hg^P_{2.5}$

393   concentrations were elevated when the RGM concentrations were low at higher wind speed (e.g.,

394   25–27 September 2015, it was cloudy these days, and there was a transitory drizzly on 26

395   September 2015) (see Figs. 2, 7, 8). On the one hand, high wind speed may increase the levels of

396   halogen atoms (Br and Cl etc.) and sea salt aerosols in the marine atmosphere, which in turn were

397   favorable to the production of RGM and formation of $Hg^P_{2.5}$ (Auzmendi-Murua et al., 2014). On

398   the other hand, high wind speed was favorable to the removal of RGM and $Hg^P_{2.5}$ in the

399   atmosphere, this was probably the reason for lower RGM and $Hg^P_{2.5}$ concentrations during 25–27

400   September as compared to those observed during 20–22 September (see Fig. 2).

401   3.5   Relationship between atmospheric Hg and meteorological parameters

402   Pearson's correlation coefficients were calculated between speciated Hg and meteorological

403   parameters to identify the relationships between them (Table 2). According to the correlation

404   analysis, the $Hg^P_{2.5}$ was significantly positively correlated with RGM. Part of the reason was that

405   RGM could be adsorbed by particulate matter under high RGM concentrations and then enhanced

406   the Hg^P concentrations. Similarly, the $Hg^P_{2.5}$ had a significantly positive correlation with GEM. On

407   the one hand, GEM and Hg^P probably originated from the same sources (including but not limited

408   to anthropogenic and oceanic sources) especially in the PRE and nearshore areas. On the other

409   hand, it was probably due to the fact that GEM could be oxidized to form RGM and then Hg^P,

410   which might be the reason for the positive but not significant correlation between RGM and GEM

411   since higher GEM level may result in higher RGM level in daytime.

412   The correlation analysis showed that the $Hg^P_{2.5}$ and RGM were all negatively correlated with

413   wind speed and RH (Table 2), and the higher wind speed was favorable to the removal of $Hg^P_{2.5}$

414   over the RGM. This is because the high wind speed might increase the RH levels and then

415   elevated wind speed and RH may accelerate the removal of $Hg^P_{2.5}$ and RGM (Cheng et al., 2014;

416   Wang et al., 2016b). Moreover, both the air temperature and PAR were positively correlated with

417   RGM and $Hg^P_{2.5}$, and a significantly positive correlation was found between PAR and RGM,

418   indicating that the role of solar radiation played on the production of RGM was more obvious than

419   that on the formation of $Hg^P_{2.5}$, which were consistent with the previous study at coastal and

420   marine sites (Mao et al., 2012).

421   3.6   Sea-air exchange of Hg^0 in the SCS

422   The spatial distributions of DGM and Hg^0 fluxes in the SCS are illustrated in Fig. 9. The DGM

423   concentrations in nearshore area (40−55 pg l^{-1}) were about twice as high as those in the open sea,

424   and this pattern was similar to our previous study conducted in the ECS (Wang et al., 2016c). The

425   DGM concentration in this study varied from 23.0 to 66.8 pg l^{-1} with a mean value of 37.1 ± 9.0

426   pg l^{-1} (Fig. 9a and Table S3), which was higher than those in other open oceans, such as the

427   Atlantic Ocean (11.6 ± 2.0 pg l^{-1}, Anderson et al., 2011), South Pacific Ocean (9−21 pg l^{-1},

428 Soerensen et al., 2014), but considerably lower than that in the Minamata Bay (116 ± 76 pg l^{-1},

429 Marumoto et al., 2015). The mean DGM concentration in the northern SCS (41.3 ± 10.9 pg l^{-1})

430 was significantly higher than that in the western SCS (33.5 ± 5.0 pg l^{-1}) (*t*-test, $p < 0.01$). The

431 reason was that DGM concentrations in the nearshore areas of the PRE and Hainan Island were

432 higher than those in the western open sea (see Fig. 9a). The DGM in surface seawater of the SCS

433 was supersaturated with a saturation of 501 % to 1468 % with a mean value of 903 ± 208 %,

434 which was approximately two thirds of that measured in the ECS (Wang et al., 2016c). The result

435 indicated that (1) the surface seawater in the SCS was supersaturated with gaseous Hg and (2) Hg^0

436 evaporated from the surface seawater to the atmosphere during our study period.

437 The sea-air exchange fluxes of Hg^0 at each station are presented in Table S3, including GEM,

438 DGM, PAR, surface seawater temperature, wind speed and saturation of Hg^0. Sea-air exchange

439 fluxes of Hg^0 in the SCS ranged from 0.40 to 12.71 ng m^{-2} h^{-1} with a mean value of 4.99 ± 3.32

440 ng m^{-2} h^{-1} (Fig. 9b and Table S3), and which was comparable to the previous measurements

441 obtained in the Mediterranean Sea, the northern SCS and West Atlantic Ocean (Andersson et al.,

442 2007; Fu et al., 2010; Soerensen et al., 2013), but lower than those in polluted marine

443 environments, such as the Minamata Bay, Tokyo Bay and YS (Narukawa et al., 2006; Ci et al.,

444 2011; Marumoto et al., 2015), while higher than those in some open sea environments, such as the

445 Baltic Sea, Atlantic Ocean and South Pacific Ocean (Kuss and Schneider, 2007; Andersson et al.,

446 2011; Kuss et al., 2011; Soerensen et al., 2014). Interestingly, we found the Hg^0 flux near the

447 station 99 were higher than those in open water as a result of higher wind speed (Table S3).

448 In order to better understand the important role of the SCS, we relate the Hg^0 flux in the SCS

449 to the global estimation, an annual sea-air flux of Hg^0 was calculated based on the assumption that

450 there was no seasonal variation in Hg^0 emission flux from the SCS. The annual emission flux of

451 Hg^0 from the SCS was estimated to be 159.6 tons yr^{-1} assuming the area of the SCS was $3.56 \times$

452 10^{12} m^2 (accounting for about 1.0 % of the global ocean area), which constituted about 5.5 % of

453 the global Hg^0 oceanic evasion (Strode et al., 2007; Soerensen et al., 2010b; UNEP, 2013). We

454 attributed the higher Hg^0 flux in the SCS to the specific location of the SCS (tropical sea) and the

455 higher DGM concentrations in the SCS (especially in the northern area). Therefore, the SCS may

456 actually play an important role in the global Hg oceanic cycle. Additionally, we found that the

457 percentage of the annual dry deposition flux of atmospheric reactive Hg to the annual evasion flux

458 of Hg^0 was approximately 18−34 %, indicating that the dry deposition of atmospheric reactive Hg

459 was an important pathway for the atmospheric Hg to the ocean.

460 **4   Conclusions**

461 During the cruise aboard the R/V *Shiyan 3* in September 2015, GEM, RGM and Hg^P were

462 determined in the MBL of the SCS. The GEM level in the SCS was comparable to the background

463 level over the global oceans due to the air masses dominantly originated from seas and oceans.

GEM concentrations were closely related to the sources and movement patterns of air masses during this cruise. Moreover, the speciated atmospheric Hg level in the PRE was significantly higher than those in the open SCS due to the anthropogenic emissions. The Hg^P concentrations in coarse particles were significantly higher than those in fine particles, and the coarse modal was the dominant size though there were three peaks for the size distribution of Hg^P in PM_{10}, indicating that most of the Hg^P_{10} originated from in situ production. There was no significant difference in GEM and $Hg^P_{2.5}$ concentrations between day and night, but RGM concentrations were significantly higher in daytime than in nighttime. RGM was positively correlated with PAR and air temperature, but negatively correlated with wind speed and RH. The DGM concentrations in nearshore areas of the SCS were higher than those in the open sea, and the surface seawater of the SCS was supersaturated with respect to Hg^0. The annual flux of Hg^0 from the SCS accounted for about 5.5 % of the global Hg^0 oceanic evasion though the area of the SCS just represents 1.0 % of the global ocean area, suggesting that the SCS plays an important role in the global Hg cycle. Additionally, the dry deposition of atmospheric reactive Hg was a momentous pathway for the atmospheric Hg to the ocean because it happens all the time.

5 Appendix A

Table A1 List of acronyms and symbols

Abbreviation	Full name
BS	Bohai Sea
YS	Yellow Sea
ECS	East China Sea
SCS	South China Sea
PRE	Pearl River Estuary
MBL	Marine boundary layer
GEM	Gaseous elemental mercury
RGM	Reactive gaseous mercury
TAM	Total atmospheric mercury
$Hg^P_{2.1}$	Particulate mercury in $PM_{2.1}$
$Hg^P_{2.5}$	Particulate mercury in $PM_{2.5}$
Hg^P_{10}	Particulate mercury in PM_{10}
DGM	Dissolved gaseous mercury

Data are available from the first author Chunjie Wang (888wangchunjie888@163.com).

References

Ahn, M. C., Kim, B., Holsen, T. M., Yi, S. M., and Han, Y. J.: Factors influencing concentrations of dissolved gaseous mercury (DGM) and total mercury (TM) in an artificial reservoir, Environ. Pollut., 158, 347–355, https://doi.org/10.1016/j.envpol.2009.08.036, 2010.

Amos, H. M., Jacob, D. J., Holmes, C. D., Fisher, J. A., Wang, Q., Yantosca, R. M., Corbitt, E. S., Galarneau, E., Rutter, A. P., Gustin, M. S., Steffen, A., Schauer, J. J., Graydon, J. A., St. Louis, V. L., Talbot, R. W., Edgerton, E. S., Zhang, Y., and Sunderland, E. M.: Gas-particle partitioning of atmopsheric Hg(II) and its effect on global mercury deposition, Atmos. Chem. Phys., 12, 591–603, https://doi.org/10.5194/acp-12-591-2012, 2012.

Andersson, M. E., Gårdfeldt, K., Wängberg, I., Sprovieri, F., Pirrone, N., and Lindqvist, O.: Seasonal and daily variation of mercury evasion at coastal and off shore sites from the Mediterranean Sea, Mar. Chem., 104, 214–226, https://doi.org/10.1016/j.marchem.2006.11.003, 2007.

Andersson, M. E., Sommar, J., Gårdfeldt, K., and Jutterström, S.: Air–sea exchange of volatile mercury in the North Atlantic Ocean, Mar. Chem., 125, 1–7, https://doi.org/10.1016/j.marchem.2011.01.005, 2011.

Angot, H., Barret, M., Magand, O., Ramonet, M., Dommergue, A.: A 2-year record of atmospheric mercury species at a background Southern Hemisphere station on Amsterdam Island, Atmos. Chem. Phys., 14, 11461–11473, https://doi.org/10.5194/acp-14-11461-2014, 2014

Ariya, P. A., Amyot, M., Dastoor, A., Deeds, D., Feinberg, A., Kos, G., Poulain, A., Ryjkov, A., Semeniuk, K., Subir, M., and Toyota, K.: Mercury Physicochemical and Biogeochemical Transformation in the Atmosphere and at Atmospheric Interfaces: A Review and Future Directions, Chem. Rev., 115, 3760–3802, https://doi.org/10.1021/cr500667e, 2015.

Athanasopoulou, E., Tombrou, M., Pandis, S. N., and Russell, A. G.: The role of sea-salt emissions and heterogeneous chemistry in the air quality of polluted coastal areas, Atmos. Chem. Phys., 8, 5755–5769, https://doi.org/10.5194/acp-8-5755-2008, 2008.

Auzmendi-Murua, I., Castillo, Á., and Bozzelli, J. W.: Mercury oxidation via chlorine, bromine, and iodine under atmospheric conditions: Thermochemistry and kinetics, J. Phys. Chem. A, 118, 2959−2975, https://doi.org/10.1021/jp412654s, 2014.

Bowman, K. L., Hammerschmidt, C. R., Lamborg, C. H., and Swarr, G.: Mercury in the North Atlantic Ocean: the U.S. Geotraces zonal and Meridional sections, Deep Sea Res. Part II, 116, 251–261, https://doi.org/10.1016/j.dsr2.2014.07.004, 2015.

521   Chand, D., Jaffe, D., Prestbo, E., Swartzendruber, P. C., Hafner, W., Weiss-Penzias, P., Kato, S., Takami, A.,

522   Hatakeyama, S., and Kajii, Y.: Reactive and particulate mercury in the Asian marine boundary layer, Atmos.

523   Environ., 42, 7988–7996, https://doi.org/10.1016/j.atmosenv.2008.06.048, 2008.

524   Cheng, I., Zhang, L., Blanchard, P., Graydon, J. A., and St. Louis, V. L.: Source-receptor relationships for speciated

525   atmospheric mercury at the remote Experimental Lakes Area, northwestern Ontario, Canada, Atmos. Chem.

526   Phys., 12, 1903–1922, https://doi.org/10.5194/acp-12-1903-2012, 2012.

527   Cheng, I., Zhang, L., Blanchard, P., Dalziel, J., Tordon, R., Huang, J., and Holsen, T. M.: Comparisons of mercury

528   sources and atmospheric mercury processes between a coastal and inland site, J. Geophys. Res., 118, 2434–2443,

529   https://doi.org/10.1002/jgrd.50169, 2013.

530   Cheng, I., Zhang, L., Mao, H., Blanchard, P., Tordon, R., and Dalziel, J.: Seasonal and diurnal patterns of speciated

531   atmospheric mercury at a coastal-rural and a coastal-urban site, Atmos. Environ., 82, 193–205,

532   https://doi.org/10.1016/j.atmosenv.2013.10.016, 2014.

533   Choi, H. D., Holsen, T. M., and Hopke, P. K.: Atmospheric mercury (Hg) in the Adirondacks: Concentrations and

534   sources, Environ. Sci. Technol., 42, 5644–5653, https://doi.org/10.1021/es7028137, 2008.

535   Ci, Z., Zhang, X., Wang, Z., Niu, Z., Diao, X., and Wang, S.: Distribution and air–sea exchange of mercury (Hg) in

536   the Yellow Sea, Atmos. Chem. Phys., 11, 2881–2892, https://doi.org/10.5194/acp-11-2881-2011, 2011.

537   Ci, Z., Wang, C., Wang, Z., and Zhang, X.: Elemental mercury (Hg(0)) in air and surface waters of the Yellow Sea

538   during late spring and late fall 2012: Concentration, spatial-temporal distribution and air/sea flux, Chemosphere,

539   119, 199–208, https://doi.org/10.1016/j.chemosphere.2014.05.064, 2015.

540   de Foy, B., Tong, Y., Yin, X., Zhang, W., Kang, S., Zhang, Q., Zhang, G., Wang, X., Schauer, J. J.: First field-based

541   atmospheric observation of the reduction of reactive mercury driven by sunlight, Atmos. Environ., 134, 27-39,

542   https://doi.org/10.1016/j.atmosenv.2016.03.028, 2016.

543   Draxler, R. R., and Rolph, G. D.: HYSPLITModel access via NOAA ARL READY Website

544   (http://www.arl.noaa.gov/ready/hysplit4.html), NOAA Air Resources Laboratory, Silver Spring, MD, 2012.

545   Engle, M. A., Tate, M. T., Krabbenhoft, D. P., Kolker, A., Olson, M. L., Edgerton, E. S., DeWild, J. F., and

546   McPherson, A. K.: Characterization and cycling of atmospheric mercury along the central US Gulf Coast, Appl.

547   Geochem., 23, 419–437, https://doi.org/10.1016/j.apgeochem.2007.12.024, 2008.

548   Feddersen, D. M., Talbot, R., Mao, H., and Sive, B. C.: Size distribution of particulate mercury in marine and

549   coastal atmospheres, Atmos. Chem. Phys., 12, 10899–10909, https://doi.org/10.5194/acp-12-10899-2012, 2012.

550   Fu, X., Feng, X., Zhang, G., Xu, W., Li, X., Yao, H., Liang, P., Li, J., Sommar, J., Yin, R., and Liu, N.: Mercury in

551   the marine boundary layer and seawater of the South China Sea: Concentrations, sea/air flux, and implication for

552   land outflow, J. Geophys. Res., 115, D06303, https://doi.org/10.1029/2009JD012958, 2010.

553   Fu, X., Feng, X., Qiu, G., Shang, L., and Zhang, H.: Speciated atmospheric mercury and its potential source in

554   Guiyang, China, Atmos. Environ., 45, 4205–4212, https://doi.org/10.1016/j.atmosenv.2011.05.012, 2011.

555   Fu, X., Feng, X., Liang, P., Deliger, Zhang, H., Ji, J., and Liu, P.: Temporal trend and sources of speciated

556   atmospheric mercury at Waliguan GAW station, Northwestern China, Atmos. Chem. Phys., 12, 1951–1964,

557   https://doi.org/10.5194/acp-12-1951-2012, 2012.

558 Gratz, L. E., Ambrose, J. L., Jaffe, D. A., Shah, V., Jaegle, L., Stutz, J., Festa, J., Spolaor, M., Tsai, C., Selin, N. E.,

559 Song, S., Zhou, X., Weinheimer, A. J., Knapp, D. J., Montzka, D. D., Flocke, F. M., Campos, T. L., Apel, E.,

560 Hornbrook, R., Blake, N. J., Hall, S., Tyndall, G. S., Reeves, M., Stechman, D., and Stell, M.: Oxidation of

561 mercury by bromine in the subtropical Pacific free troposphere, Geophys. Res. Lett., 42, 10494–10502,

562 https://doi.org/10.1002/2015GL066645, 2015.

563 Giorgi, F.: Dry deposition velocities of atmospheric aerosols as inferred by applying a particle dry deposition

564 parameterisation   to   a   general   circulation   model,   Tellus,   40B,   23–41,

565 https://doi.org/10.1111/j.1600-0889.1988.tb00210.x, 1988.

566 Gustin, M. S., Huang, J., Miller, M. B., Peterson, C., Jaffe, D. A., Ambrose, J., Finley, B. D., Lyman, S. N., Call,

567 K., Talbot, R., Feddersen, D., Mao, H., and Lindberg, S. E.: Do we understand what the mercury speciation

568 instruments are actually measuring? Results of RAMIX, Environ. Sci. Technol., 47, 7295–7306,

569 https://doi.org/10.1021/es3039104, 2013.

570 Hedgecock, I. and Pirrone, N.: Mercury and photochemistry in the marine boundary layer-modelling studies

571 suggest the in situ production of reactive gas phase mercury, Atmos. Environ., 35, 3055–3062,

572 https://doi.org/10.1016/S1352-2310(01)00109-1, 2001.

573 Holmes, C. D., Jacob, D. J., and Yang, X.: Global lifetime of elemental mercury against oxidation by atomic

574 bromine in the free troposphere, Geophys. Res. Lett., 33, L20808, https://doi.org/10.1029/2006gl027176, 2006.

575 Holmes, C. D., Jacob, D. J., Mason, R. P., and Jaffe, D. A.: Sources and deposition of reactive gaseous mercury in

576 the marine atmosphere, Atmos. Environ., 43, 2278–2285, https://doi.org/10.1016/j.atmosenv.2009.01.051, 2009.

577 Holmes, C. D., Jacob, D. J., Corbitt, E. S., Mao, J., Yang, X., Talbot, R., and Slemr, F.: Global atmospheric model

578 for mercury including oxidation by bromine atoms, Atmos. Chem. Phys., 10, 12037−12057,

579 https://doi.org/10.5194/acp-10-12037-2010, 2010.

580 Horowitz, H. M., Jacob, D. J., Zhang, Y., Dibble, T. S., Slemr, F., Amos, H. M., Schmidt, J. A., Corbitt, E. S.,

581 Marais, E. A., and Sunderland, E. M.: A new mechanism for atmospheric mercury redox chemistry: implications

582 for the global mercury budget, Atmos. Chem. Phys., 17, 6353-6371, https://doi.org/10.5194/acp-17-6353-2017,

583 2017.

584 Horvat, M., Kotnik, J., Logar, M., Fajon, V., Zvonarić, T., and Pirrone, N.: Speciation of mercury in surface and

585 deep-sea   waters   in   the   Mediterranean   Sea,   Atmos.   Environ.,   37,   S93–S108,

586 https://doi.org/10.1016/S1352-2310(03)00249-8, 2003.

587 Howard, D., Nelson, P. F., Edwards, G. C., Morrison, A. L., Fisher, J. A., Ward, J., Harnwell, J., van der Schoot, M.,

588 Atkinson, B., Chambers, S. D., Griffiths, A. D., Werczynski, S., and Williams, A. G.: Atmospheric mercury in

589 the Southern Hemisphere tropics: seasonal and diurnal variations and influence of inter-hemispheric transport,

590 Atmos. Chem. Phys., 17, 11623-11636, https://doi.org/10.5194/acp-17-11623-2017, 2017.

591 Huang, J., Miller, M. B., Edgerton, E., and Sexauer Gustin, M.: Deciphering potential chemical compounds of

592 gaseous   oxidized   mercury   in   Florida,   USA,   Atmos.   Chem.   Phys.,   17,   1689-1698,

593 https://doi.org/10.5194/acp-17-1689-2017, 2017.

594 Kim, S. H., Han, Y. J., Holsen, T. M., and Yi, S. M.: Characteristics of atmospheric speciated mercury

concentrations (TGM, Hg(II) and Hg(p)) in Seoul, Korea, Atmos. Environ., 43, 3267–3274, https://doi.org/10.1016/j.atmosenv.2009.02.038, 2009.

Kim, P. R., Han, Y. J., Holsen, T. M., and Yi, S. M.: Atmospheric particulate mercury: Concentrations and size distributions, Atmos. Environ., 61, 94–102, https://doi.org/10.1016/j.atmosenv.2012.07.014, 2012.

Kuss, J.: Water–air gas exchange of elemental mercury: An experimentally determined mercury diffusion coefficient for Hg^0 water–air flux calculations, Limnol. Oceanogr., 59, 1461–1467, https://doi.org/10.4319/lo.2014.59.5.1461, 2014.

Kuss, J., and Schneider, B.: Variability of the gaseous elemental mercury sea-air flux of the Baltic Sea, Environ. Sci. Technol., 41, 8018–8023, https://doi.org/10.1021/es0716251, 2007.

Kuss, J., Zülicke, C., Pohl, C., and Schneider, B.: Atlantic mercury emission determined from continuous analysis of the elemental mercury sea-air concentration difference within transects between 50°N and 50°S, Global Biogeochem. Cycles, 25, GB 3021, https://doi.org/10.1029/2010GB003998, 2011.

Kuss, J., Krüger, S., Ruickoldt, J., and Wlost, K.-P.: High-resolution measurements of elemental mercury in surface water for an improved quantitative understanding of the Baltic Sea as a source of atmospheric mercury, Atmos. Chem. Phys., 18, 4361-4376, https://doi.org/10.5194/acp-18-4361-2018, 2018.

Landis, M. S., Stevens, R. K., Schaedlich, F., and Prestbo, E. M.: Development and characterization of an annular denuder methodology for the measurement of divalent inorganic reactive gaseous mercury in ambient air, Environ. Sci. Technol., 36, 3000–3009, https://doi.org/10.1021/es015887t, 2002.

Laurier, F. J. G., Mason, R. P., Whalin, L., and Kato, S.: Reactive gaseous mercury formation in the North Pacific Ocean's marine boundary layer: A potential role of halogen chemistry, J. Geophys. Res., 108, 4529, https://doi.org/10.1029/2003JD003625, 2003.

Laurier, F., and Mason, R.: Mercury concentration and speciation in the coastal and open ocean boundary layer, J. Geophys. Res., 112, D06302, https://doi.org/10.1029/2006JD007320, 2007.

Lee, G.-S., Kim, P.-R., Han, Y.-J., Holsen, T. M., Seo, Y.-S., and Yi, S.-M.: Atmospheric speciated mercury concentrations on an island between China and Korea: sources and transport pathways, Atmos. Chem. Phys., 16, 4119-4133, https://doi.org/10.5194/acp-16-4119-2016, 2016.

Lindberg, S. E., Brooks, S., Lin, C. J., Scott, K. J., Landis, M. S., Stevens, R. K., Goodsite, M., and Richter, A.: Dynamic oxidation of gaseous mercury in the Arctic troposphere at polar sunrise, Environ. Sci. Technol., 36, 1245–1256, https://doi.org/10.1021/es0111941, 2002.

Liss, P. W., and Slater, P. G.: Flux of gases across the air-sea interface, Nature, 247, 181–184, https://doi.org/10.1038/247181a0, 1974.

Liu, B., Keeler, G. J., Dvonch, J. T., Barres, J. A., Lynam, M. M., Marsik, F. J., and Morgan, J. T.: Temporal variability of mercury speciation in urban air, Atmos. Environ., 41, 1911–1923, https://doi.org/10.1016/j.atmosenv.2006.10.063, 2007.

Liu, B., Keeler, G. J., Dvonch, J. T., Barres, J. A., Lynam, M. M., Marsik, F. J., and Morgan, J. T.: Urban-rural differences in atmospheric mercury speciation, Atmos. Environ., 44, 2013–2023, https://doi.org/10.1016/j.atmosenv.2010.02.012, 2010.

632 Liu, N., Qiu, G., Landis, M., Feng, X., Fu, X., and Shang, L.: Atmospheric mercury species measured in Guiyang,

633 Guizhou province, southwest China, Atmos. Res., 100, 93–102, https://doi.org/10.1016/j.atmosres.2011.01.002,

634 2011.

635 Mamane, Y., Perrino, C., Yossef, O., and Catrambone, M.: Source characterization of fine and coarse particles at

636 the East mediterranean coast, Atmos. Environ., 42, 6114–6130, doi:10.1016/j.atmosenv.2008.02.045, 2008.

637 Mao, H., Talbot, R., Hegarty, J., and Koermer, J.: Speciated mercury at marine, coastal, and inland sites in New

638 England – Part 2: Relationships with atmospheric physical parameters, Atmos. Chem. Phys., 12, 4181–4206,

639 https://doi.org/10.5194/acp-12-4181-2012, 2012.

640 Mao, H., Cheng, I., and Zhang, L.: Current understanding of the driving mechanisms for spatiotemporal variations

641 of   atmospheric   speciated   mercury: a   review,   Atmos.   Chem.   Phys.,   16,   12897–12924,

642 https://doi.org/10.5194/acp-16-12897-2016, 2016.

643 Mao, H., Hall, D., Ye, Z., Zhou, Y., Felton, D., and Zhang, L.: Impacts of large-scale circulation on urban ambient

644 concentrations of gaseous elemental mercury in New York, USA, Atmos. Chem. Phys., 17, 11655–11671,

645 https://doi.org/10.5194/acp-17-11655-2017, 2017.

646 Marumoto, K., and Imai, S.: Determination of dissolved gaseous mercury in seawater of Minamata Bay and

647 estimation   for   mercury   exchange   across   air–sea   interface,   Mar.   Chem.,   168,   9–17,

648 https://doi.org/10.1016/j.marchem.2014.09.007, 2015.

649 Mason, R. P., Choi, A. L., Fitzgerald, W. F., Hammerschmidt, C. R., Lamborg, C. H., Soerensen, A. L., and

650 Sunderland, E. M.: Mercury biogeochemical cycling in the ocean and policy implications, Environ. Res., 119,

651 101–117, doi:10.1016/j.envres.2012.03.013, 2012.

652 Mason, R. P., Hammerschmidt, C. R., Lamborg, C. H., Bowman, K. L., Swarr, G. J., and Shelley, R. U.: The air-sea

653 exchange of mercury in the low latitude Pacific and Atlantic Oceans, Deep Sea Res. Part I, 122, 17–28,

654 https://doi.org/10.1016/j.dsr.2017.01.015, 2017.

655 Narukawa, M., Sakata, M., Marumoto, K., and Asakura, K.: Air-sea exchange of mercury in Tokyo Bay, J.

656 Oceanogr., 62, 249–257, https://doi.org/10.1007/s10872-006-0049-3, 2006.

657 Nho-Kim, E. Y., Michou, M., and Peuch, V. H.: Parameterization of size-dependent particle dry deposition

658 velocities for global modeling, Atmos. Environ., 38, 1933–1942, https://doi.org/10.1016/j.atmosenv.2004.01.002,

659 2004.

660 Poissant, L., Pilote, M., Xu, X., Zhang, H. and Beauvais C.: Atmospheric mercury speciation and deposition in the

661 Bay St. François wetlands, J. Geophys. Res., 109, D11301, https://doi.org/10.1029/2003JD004364, 2004.

662 Pryor, S. C., and Sorensen, L. L.: Nitric acid-sea salt reactions: Implications for nitrogen deposition to water

663 surfaces, J. Appl. Meteorol., 39, 725–731, https://doi.org/10.1175/1520-0450-39.5.725, 2000.

664 Radke, L. F., Friedli, H. R., and Heikes, B. G.: Atmospheric mercury over the NE Pacific during spring 2002:

665 Gradients, residence time, upper troposphere lower stratosphere loss, and long-range transport, J. Geophys. Res.,

666 112, D19305, https://doi.org/10.1029/2005JD005828, 2007.

667 Read, K. A., Neves, L. M., Carpenter, L. J., Lewis, A. C., Fleming, Z. L., and Kentisbeer, J.: Four years

668 (2011–2015) of total gaseous mercury measurements from the Cape Verde Atmospheric Observatory, Atmos.

669   Chem. Phys., 17, 5393-5406, https://doi.org/10.5194/acp-17-5393-2017, 2017.

670   Rutter, A. P., and Schauer, J. J.: The effect of temperature on the gas–particle partitioning of reactive mercury in

671   atmospheric aerosols, Atmos. Environ., 41, 8647–8657, https://doi.org/10.1016/j.atmosenv.2007.07.024, 2007.

672   Sander, R., Keene, W. C., Pszenny, A. A. P., Arimoto, R., Ayers, G. P., Baboukas, E., Cainey, J. M., Crutzen, P. J.,

673   Duce, R. A., Hönninger, G., Huebert, B. J., Maenhaut, W., Mihalopoulos, N., Turekian, V. C., and Van Dingenen,

674   R., Inorganic bromine in the marine boundary layer: a critical review, Atmos. Chem. Phys., 3, 1301–1336,

675   https://doi.org/10.5194/acp-3-1301-2003, 2003.

676   Schroeder, W. H., and Munthe, J.: Atmospheric mercury – An overview, Atmos. Environ., 32, 809–822,

677   https://doi.org/10.1016/S1352-2310(97)00293-8, 1998.

678   Selin, N. E., Jacob, D. J., Park, R. J., Yantosca, R. M., Strode, S., Jaeglé, L., and Jaffe, D.: Chemical cycling and

679   deposition of atmospheric mercury: Global constraints from observations, J. Geophys. Res., 112, D02308,

680   https://doi.org/10.1029/2006JD007450, 2007.

681   Shah, V., Jaeglé, L., Gratz, L. E., Ambrose, J. L., Jaffe, D. A., Selin, N. E., Song, S., Campos, T. L., Flocke, F. M.,

682   Reeves, M., Stechman, D., Stell, M., Festa, J., Stutz, J., Weinheimer, A. J., Knapp, D. J., Montzka, D. D.,

683   Tyndall, G. S., Apel, E. C., Hornbrook, R. S., Hills, A. J., Riemer, D. D., Blake, N. J., Cantrell, C. A., and

684   Mauldin III, R. L.: Origin of oxidized mercury in the summertime free troposphere over the southeastern US,

685   Atmos. Chem. Phys., 16, 1511-1530, https://doi.org/10.5194/acp-16-1511-2016, 2016.

686   Sheu, G. R., and Mason, R. P.: An examination of the oxidation of elemental mercury in the presence of halide

687   surfaces, J. Atmos. Chem., 48, 107–130, https://doi.org/10.1023/B:JOCH.0000036842.37053.e6, 2004.

688   Slemr, F., Angot, H., Dommergue, A., Magand, O., Barret, M., Weigelt, A., Ebinghaus, R., Brunke, E.-G.,

689   Pfaffhuber, K. A., Edwards, G., Howard, D., Powell, J., Keywood, M., and Wang, F.: Comparison of mercury

690   concentrations measured at several sites in the Southern Hemisphere, Atmos. Chem. Phys., 15, 3125-3133,

691   https://doi.org/10.5194/acp-15-3125-2015, 2015.

692   Soerensen, A. L., Skov, H., Jacob, D. J., Soerensen, B. T., and Johnson, M. S.: Global concentrations of gaseous

693   elemental mercury and reactive gaseous mercury in the marine boundary layer, Environ. Sci. Technol., 44,

694   7425–7430, https://doi.org/10.1021/es903839n, 2010a.

695   Soerensen, A. L., Sunderland, E. M., Holmes, C. D., Jacob, D. J., Yantosca, R. M., Skov, H., Christensen, J. H.,

696   Strode, S. A., and Mason, R. P.: An improved global model for air-sea exchange of mercury: high concentrations

697   over the North Atlantic, Environ. Sci. Technol., 44, 8574–8580, https://doi.org/10.1021/es102032g, 2010b.

698   Soerensen, A. L., Mason, R. P., Balcom, P. H., and Sunderland, E. M.: Drivers of surface ocean mercury

699   concentrations and air–sea exchange in the west Atlantic Ocean, Environ. Sci. Technol., 47, 7757–7765,

700   https://doi.org/10.1021/es401354q, 2013.

701   Soerensen, A. L., Mason, R. P., Balcom, P. H., Jacob, D. J., Zhang, Y., Kuss, J., and Sunderland, E. M.: Elemental

702   mercury concentrations and fluxes in the tropical atmosphere and ocean, Environ. Sci. Technol., 48,

703   11312–11319, https://doi.org/10.1021/es503109p, 2014.

704   Sprovieri, F., Pirrone, N., Gärdfeldt, K., and Sommar, J.: Mercury speciation in the marine boundary layer along a

705   6000   km   cruise   path   around   the   Mediterranean   Sea,   Atmos.   Environ.,   37,   S63–S71,

https://doi.org/10.1016/S1352-2310(03)00237-1, 2003.

Sprovieri, F., and Pirrone, N.: Spatial and temporal distribution of atmospheric mercury species over the Adriatic Sea, Environ. Fluid Mech., 8, 117–128, https://doi.org/10.1007/s10652-007-9045-4, 2008.

Sprovieri, F., Hedgecock, I. M., and Pirrone, N.: An investigation of the origins of reactive gaseous mercury in the Mediterranean marine boundary layer, Atmos. Chem. Phys., 10, 3985–3997, https://doi.org/10.5194/acp-10-3985-2010, 2010.

Steffen, A., Lehnherr, I., Cole, A., Ariya, P., Dastoor, A., Durnford, D., Kirk, J., and Pilote, M.: Atmospheric mercury measurements in the Canadian Arctic Part 1: A review of recent field measurements, Sci. Total Environ., 509–510, 3–15, https://doi.org/10.1016/j.scitotenv.2014.10.109, 2015.

Strode, S. A., Jaeglé, L., Selin, N. E., Jacob, D. J., Park, R. J., Yantosca, R. M., Mason, R. P., and Slemr, F.: Air-sea exchange in the global mercury cycle, Global Biogeochem. Cycles, 21, GB1017, https://doi.org/10.1029/2006GB002766, 2007.

Tseng, C. M., Liu, C. S., and Lamborg, C.: Seasonal changes in gaseous elemental mercury in relation to monsoon cycling over the northern South China Sea, Atmos. Chem. Phys., 12, 7341–7350, https://doi.org/10.5194/acp-12-7341-2012, 2012.

UNEP: Global Mercury Assessment: Sources, Emissions, Releases and Environmental Transport, UNEP Chemicals Branch, Geneva, Switzerland, 2013.

Valente, R. J., Shea, C., Humes, K. L., and Tanner, R. L.: Atmospheric mercury in the Great Smoky Mountains compared to regional and global levels, Atmos. Environ., 41, 1861–1873, https://doi.org/10.1016/j.atmosenv.2006.10.054, 2007.

Wang, Y. Q., Zhang, X. Y., and Draxler, R. R.: TrajStat: GIS-based software that uses various trajectory statistical analysis methods to identify potential sources from long-term air pollution measurement data, Environ. Model. Softw., 28, 938–939, https://doi.org/10.1016/j.envsoft.2009.01.004, 2009.

Wang, S., Schmidt, J. A., Baidar, S., Coburn, S., Dix, B., Koenig, T. K., Apel, E., Bowdalo, D., Campos, T. L., Eloranta, E., Evans, M. J., DiGangi, J. P., Zondlo, M. A., Gao, R. S., Haggerty, J. A., Hall, S. R., Hornbrook, R. S., Jacob, D., Morley, B., Pierce, B., Reeves, M., Romashkin, P., ter Schure, A., and Volkamer, R.: Active and widespread halogen chemistry in the tropical and subtropical free troposphere, Proc. Natl. Acad. Sci. U.S.A., 112, 9281–9286, https://doi.org/10.1073/pnas.1505142112, 2015.

Wang, C., Wang, Z., Ci, Z., Zhang, X., and Tang, X.: Spatial-temporal distributions of gaseous element mercury and particulate mercury in the Asian marine boundary layer, Atmos. Environ., 126, 107–116, https://doi.org/10.1016/j.atmosenv.2015.11.036, 2016a.

Wang, C., Ci, Z., Wang, Z., Zhang, X., and Guo, J.: Speciated atmospheric mercury in the marine boundary layer of the Bohai Sea and Yellow Sea, Atmos. Environ., 131, 360–370, https://doi.org/10.1016/j.atmosenv.2016.02.021, 2016b.

Wang, C., Ci, Z., Wang, Z., and Zhang, X.: Air-sea exchange of gaseous mercury in the East China Sea, Environ. Pollut., 212, 535–543, https://doi.org/10.1016/j.envpol.2016.03.016, 2016c.

Wanninkhof, R.: Relationship between wind speed and gas exchange over the ocean, J. Geophys. Res., 97,

743 7373–7382, https://doi.org/10.1029/92JC00188, 1992.

744 Witt, M. L. I., Mather, T. A., Baker, A. R., De Hoog, J. C. M., and Pyle, D. M.: Atmospheric trace metals over the

745 south-west Indian Ocean: Total gaseous mercury, aerosol trace metal concentrations and lead isotope ratios, Mar.

746 Chem., 121, 2–16, https://doi.org/10.1016/j.marchem.2010.02.005, 2010.

747 Xu, L., Chen, J., Yang, L., Niu, Z., Tong, L., Yin, L., and Chen, Y.: Characteristics and sources of atmospheric

748 mercury speciation in a coastal city, Xiamen, China, Chemosphere, 119, 530–539,

749 https://doi.org/10.1016/j.chemosphere.2014.07.024, 2015.

750 Ye, Z., Mao, H., Lin, C.-J., and Kim, S. Y.: Investigation of processes controlling summertime gaseous elemental

751 mercury oxidation at midlatitudinal marine, coastal, and inland sites, Atmos. Chem. Phys., 16, 8461–8478,

752 https://doi.org/10.5194/acp-16-8461-2016, 2016.

753 Zhu, J., Wang, T., Talbot, R., Mao, H., Yang, X., Fu, C., Sun, J., Zhuang, B., Li, S., Han, Y., and Xie, M.:

754 Characteristics of atmospheric mercury deposition and size-fractionated particulate mercury in urban Nanjing,

755 China, Atmos. Chem. Phys., 14, 2233–2244, https://doi.org/10.5194/acp-14-2233-2014, 2014.

756

757 **Figures and Tables**
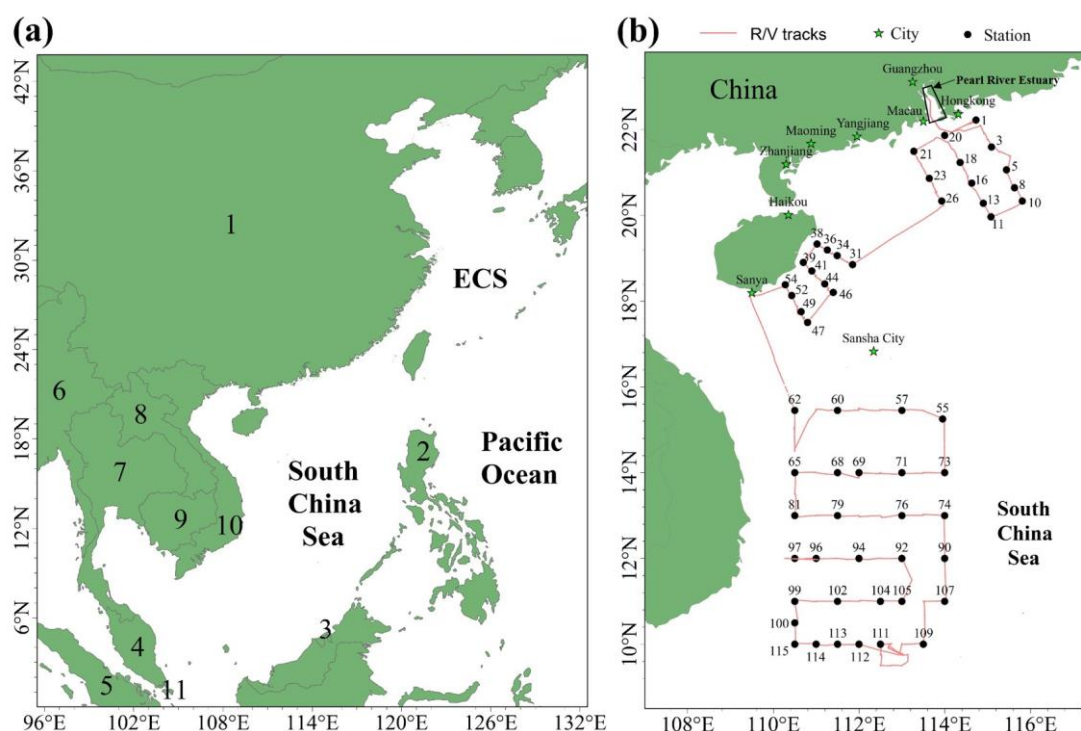
759 **Figure 1.** Map of the South China Sea (a) (1: China, 2: Philippines, 3: Brunei, 4: Malaysia, 5:
760 Indonesia, 6: Myanmar, 7: Thailand, 8: Laos, 9: Cambodia, 10: Vietnam, 11: Singapore). The
761 locations of the Pearl River Estuary (PRE), DGM sampling stations and R/V tracks (b). It should
762 be noted that the black solid points represent the sampling stations, and the number near the black
763 solid point represents the name of the station.

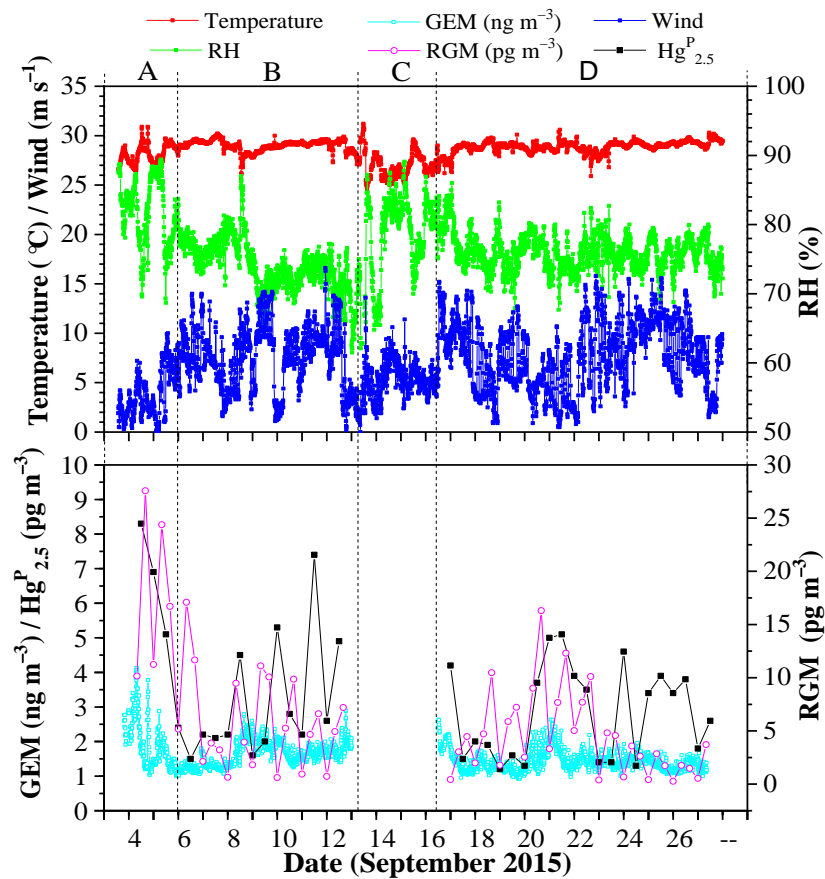**Figure 2.** Time (local time) series of GEM, $Hg^P_{2.5}$, RGM and some meteorological parameters, including relative humidity (RH), air temperature and wind speed ("A" represents the data measured in the PRE, "B" represents the data measured in the northern SCS, "C" represents the data obtained in the port of Sanya, "D" represents the data measured in the western SCS). It was rainy day on the days of 8 and 26 September 2015.

770
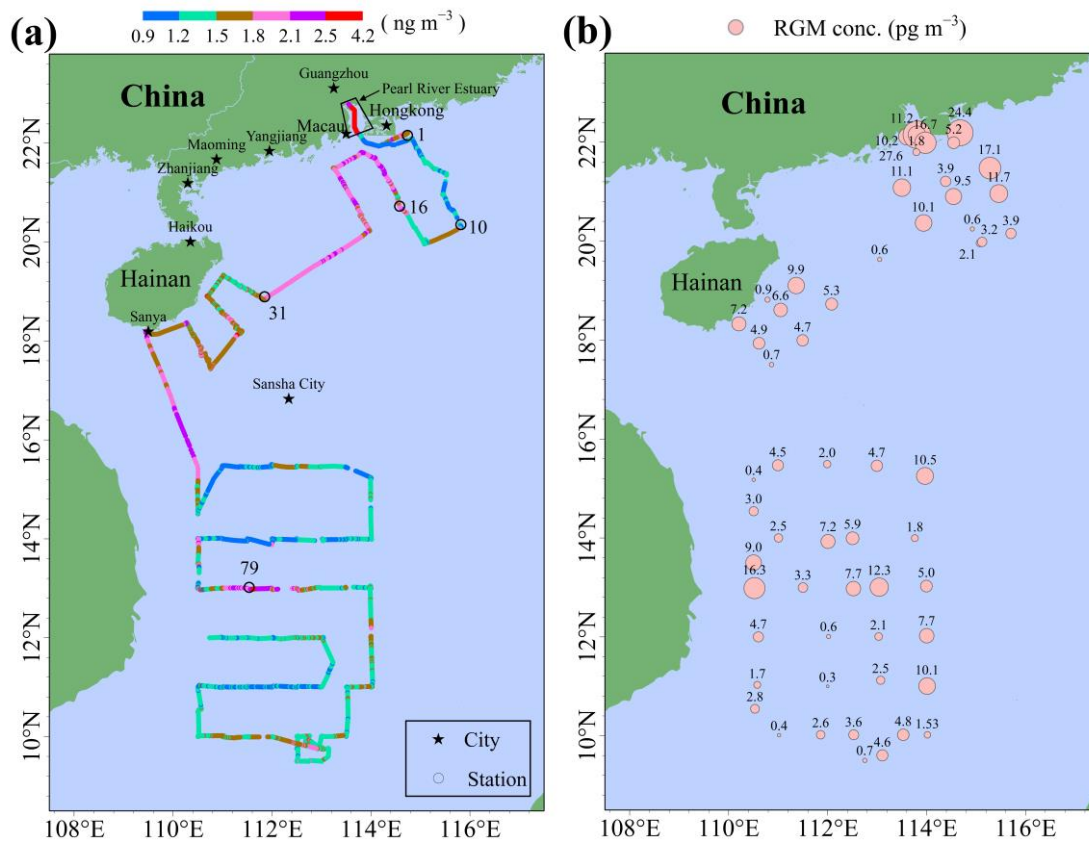
Figure 3. The concentrations and spatial distributions of GEM (a) and RGM (b) in the MBL of the

772 SCS.

773
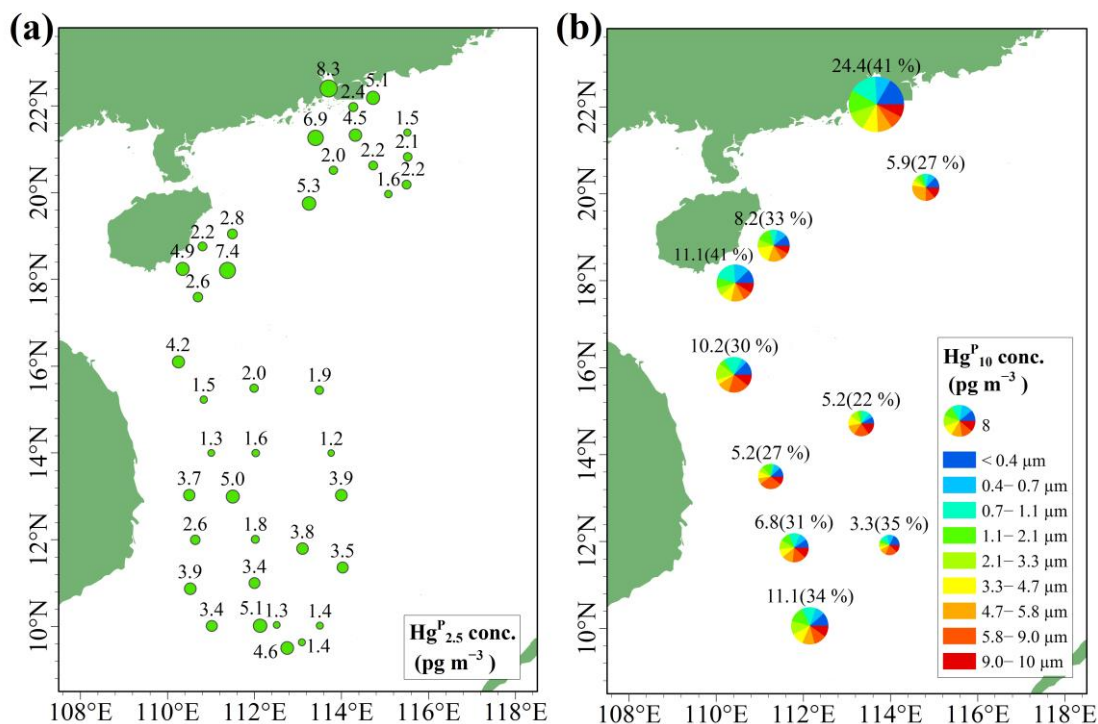
Figure 4. Spatial distributions of $Hg^P_{2.5}$ (a) and Hg^P_{10} ($Hg^P_{2.1}/Hg^P_{10}$ ratio) (b) in the MBL of the

775 SCS. $Hg^P_{2.5}$, $Hg^P_{2.1}$ and Hg^P_{10} denote the Hg^P in $PM_{2.5}$, $PM_{2.1}$ and PM_{10}, respectively.

24
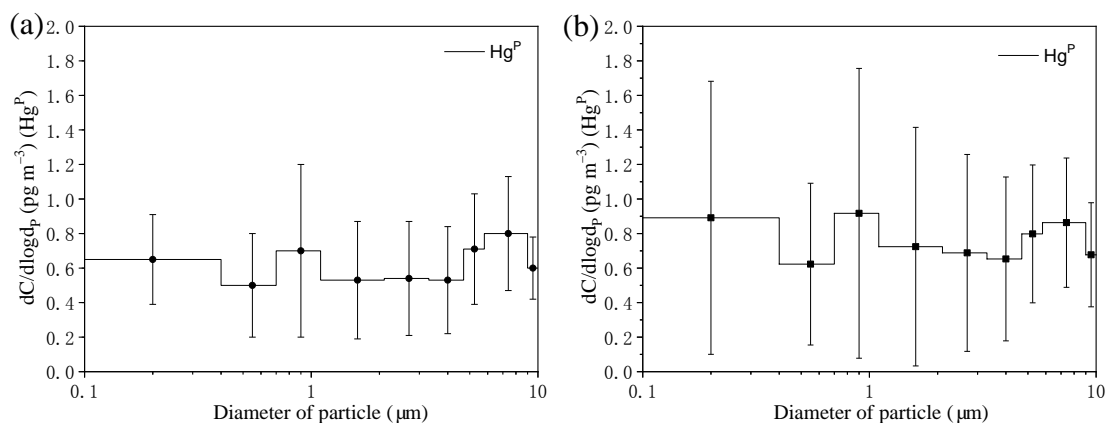
Figure 5. Size distributed concentrations of Hg^P (PM$_{10}$) in the MBL of the SCS, (a) represents all the data excepting the measurements in the PRE; (b) represents all the data. The data shown are the mean and standard error.
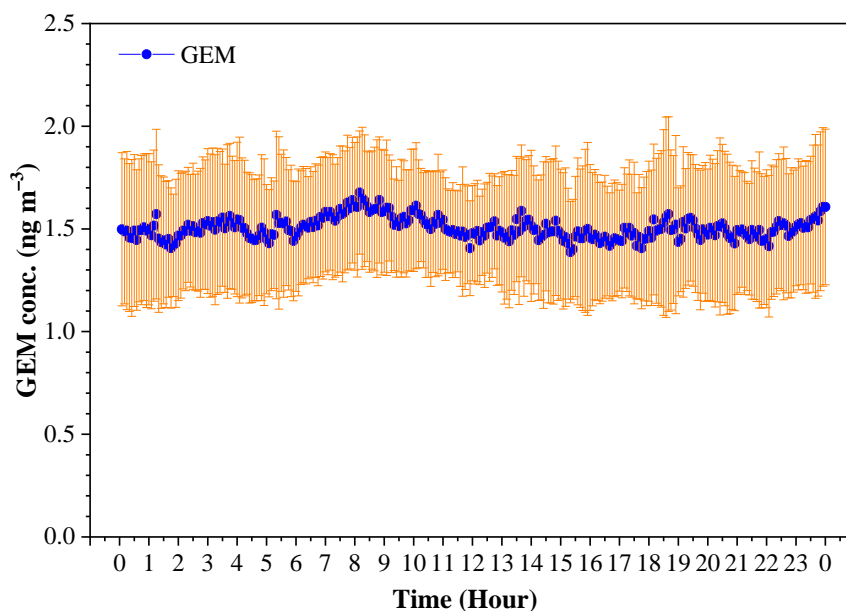
Figure 6. Diurnal variation of GEM concentration (mean ±SD) over the SCS.

782
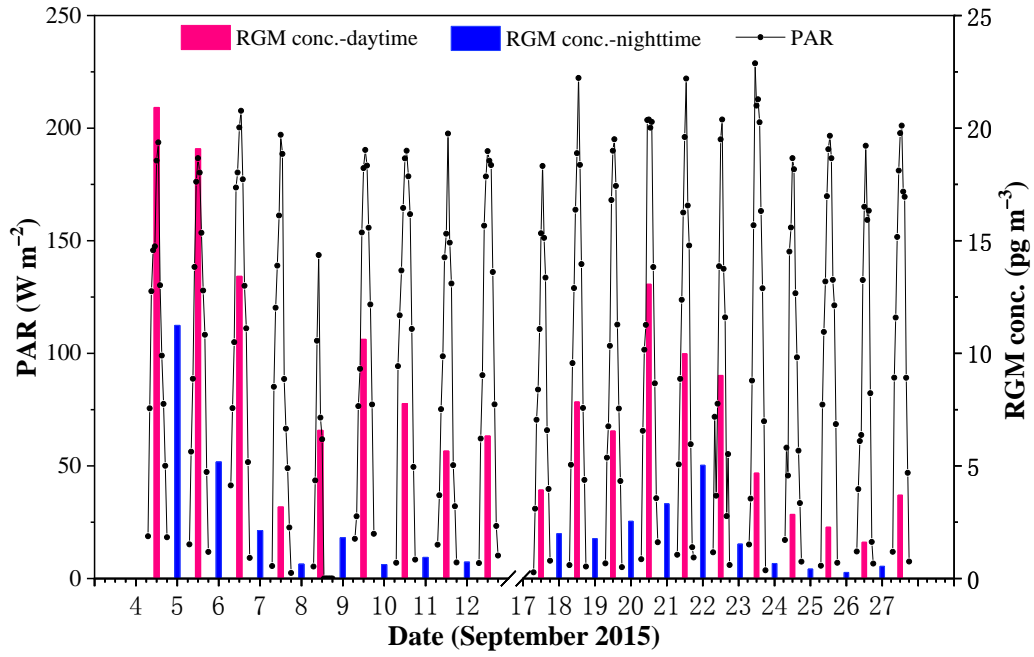
Figure 7. Daily variation of RGM concentration over the SCS.

784

785

Figure 8. Daily variation of $Hg^P_{2.5}$ in the MBL of the SCS. The light gray area represents the data

in the PRE, while the light magenta area represents the data in the nearshore area of the Hainan

Island.

Figure 9. DGM concentrations (a) and sea-air exchange flux of Hg^0 (b) in the SCS.

Table 1. The GEM, $Hg^P_{2.5}$ and RGM concentrations in this study and other literature.

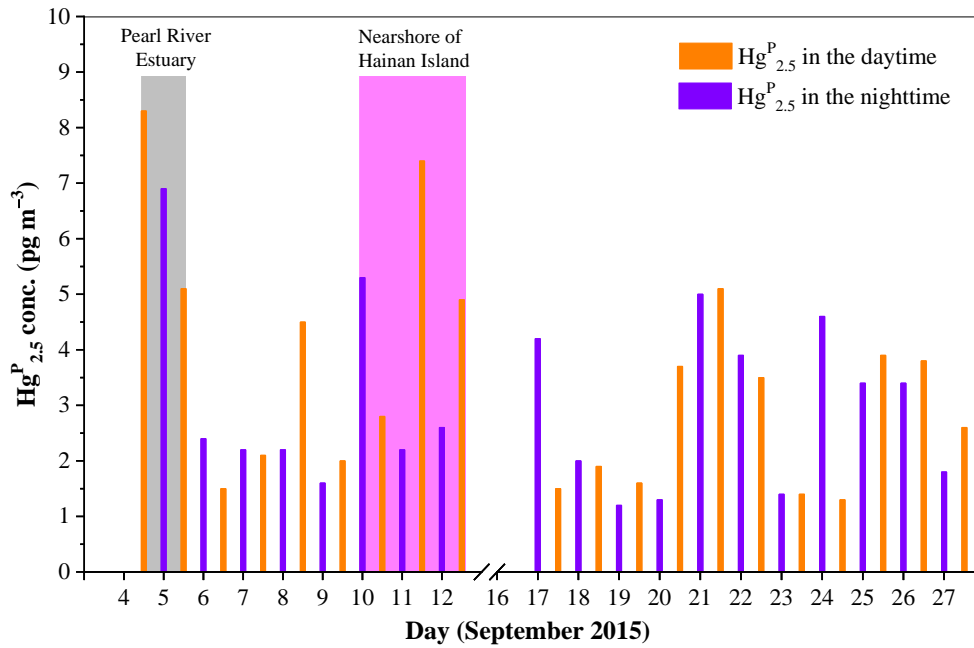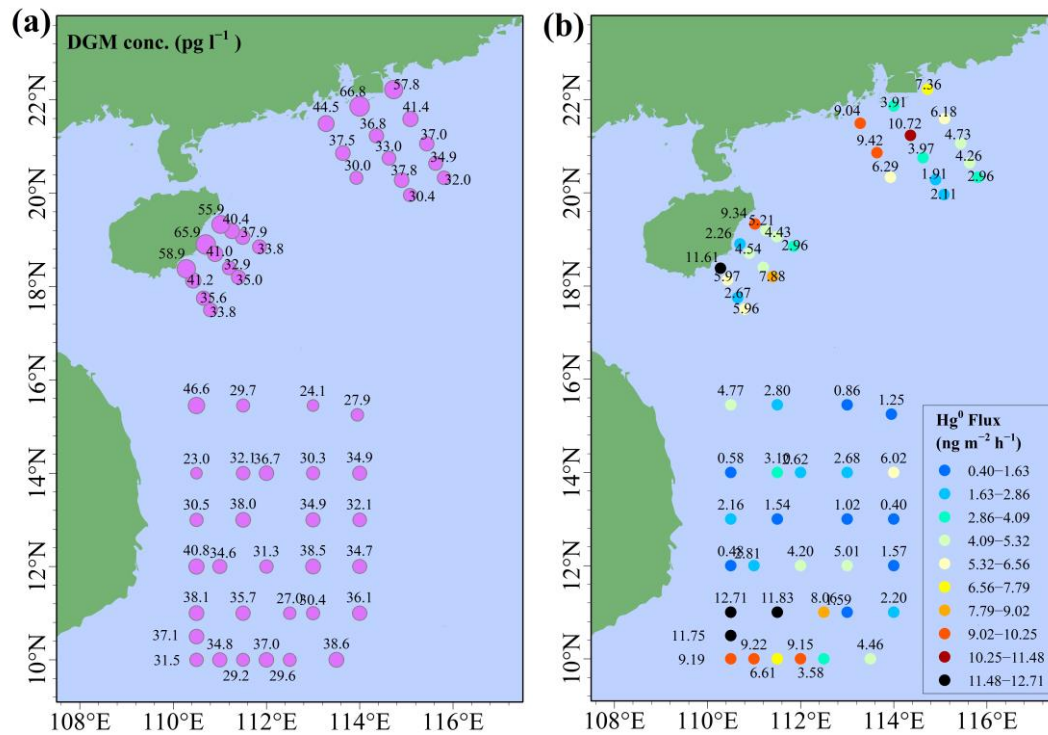| Location		Classification	Sampling time	GEM (ng m^{-3})	Hg$^P_{2.5}$ (pg m^{-3})	RGM (pg m^{-3})	Reference
China	SCS	Sea	2015	1.52 ±0.32	3.2 ±1.8	6.1 ±5.8	This study
	BS and YS	Sea	2014 (Spring)	2.03 ±0.72	11.3 ±18.5	2.5 ±1.7	Wang et al., 2016a, b
	BS and YS	Sea	2014 (Fall)	2.09 ±1.58	9.0 ±9.0	4.3 ±2.5	Wang et al., 2016a, b
	YS	Sea	2010 (Summer)	2.61 ±0.50	NA[a]	NA	Ci et al., 2011
	YS	Sea	2012 (Spring)	1.86 ±0.40	NA	NA	Ci et al., 2015
	YS	Sea	2012 (Fall)	1.84 ±0.50	NA	NA	Ci et al., 2015
	ECS	Sea	2013 (Summer)	1.61 ±0.32	NA	NA	Wang et al., 2016c
	ECS	Sea	2013 (Fall)	2.20 ±0.58	NA	NA	Wang et al., 2016c
	Northern SCS	Sea	2007	2.62 ±1.13	NA	NA	Fu et al., 2010
	Northern SCS	Sea	2003−2005	2.8 −5.7	NA	NA	Tseng et al., 2012
	Nam Co	lake	2014−2015	0.95 ±0.37	0.85 ±2.91	49.0 ±60.3	de Foy et al., 2016
	Xiamen	Coastal urban	2012−2013	3.50	61.05	174.41	Xu et al., 2015
Japan	Okinawa Island	Ocean	2004	2.04 ±0.38	3.0 ±2.5	4.5 ±5.4	Chand et al., 2008
Korea	Seoul	Urban	2005−2006	3.22 ±2.10	23.9 ±19.6	27.2 ±19.3	Kim et al., 2009
USA	Weeks Bay	Coast	2005−2006	1.6 ±0.3	2.7 ±3.4	4.0 ±7.5	Engle et al., 2008
Canada	Ontario Lake	Remote area	2005−2006	1.57 ±0.22	4.42 ±3.67	0.99 ±1.89	Cheng et al., 2012
	Nova Scotia	Coast	2010−2011	1.67 ±1.01	2.32 ±3.09	2.07 ±3.35	Cheng et al., 2013
	Nova Scotia	Coast-rural	2010−2011	1.38 ±0.20	3.5 ±4.5	0.4 ±1.0	Cheng et al., 2014
Australia	ATARS[b]	Coast	2014-2015	0.95 ±0.12	NA	NA	Howard et al., 2017
South-west India Ocean		Ocean	2007	1.24 ±0.06	NA	NA	Witt et al., 2010
North Atlantic Ocean		Ocean	2003	1.63 ±0.08	NA	5.9 ±4.9	Laurier et al., 2007
West Atlantic Ocean		Ocean	2008−2010	1.4−1.5	NA	NA	Soerensen et al., 2013
North Pacific Ocean		Ocean	2002	2.5	NA	9.5	Laurier et al., 2003
Pacific Ocean		Ocean	2011	1.15−1.32	NA	NA	Soerensen et al., 2014
Mediterranean Sea		Sea	2000	1.9 ±1.0	NA	7.9	Sprovieri et al., 2003
Global Ocean		Ocean	2006−2007	1.53 ±0.58	NA	3.1 ±11.0	Soerensen et al., 2010a
Adriatic Sea		Ocean	2004	1.6 ±0.4	4.5 ±8.0	6.7 ±11.7	Sprovieri and Pirrone, 2008
Amsterdam Island		Ocean	2012−2013	1.03 ±0.08	0.67	0.34	Angot et al., 2014

[a] NA: No data available.

[b] ATARS: Australian Tropical Atmospheric Research Station.

794 **Table 2.** Correlation coefficients for speciated atmospheric Hg and meteorological parameters (one asterisk

795 denotes significant correlation in $p < 0.05$, double asterisks denotes significant correlation in $p < 0.01$).

Speciation	GEM		RGM		$Hg^P_{2.5}$		Wind speed		Air temperature		RH		PAR	
	p	r	p	r	p	r	p	r	p	r	p	r	p	r
RGM	0.069	0.294			< 0.01	0.453^{**}	0.123	−0.251	0.053	0.313	0.065	−0.299	< 0.01	0.638^{**}
$Hg^P_{2.5}$	< 0.01	0.539^{**}	< 0.01	0.453^{**}			0.037	$−0.335^{*}$	0.621	0.082	0.434	−0.129	0.432	0.130

796

1 *Supplement of*

Speciated atmospheric mercury and sea-air exchange of

gaseous mercury in the South China Sea

4 Chunjie Wang[1], Zhangwei Wang[1], Fan Hui[2], Xiaoshan Zhang[1]

5 [1] Research Center for Eco-Environmental Sciences, Chinese Academy of Sciences, 18 Shuangqing Road, Beijing,

6 China

7 [2] China University of Petroleum (Beijing), 18 Fuxue Road, Beijing, China

8 Correspondence to: Xiaoshan Zhang (zhangxsh@rcees.ac.cn)

9
10
11
12
13
14
15
16
17
18
19
20
21
22
23
24
25
26
27
28
29
30
31
32
33
34
35
36
37
38
39

Table S1. The concentration (pg m^{-3}) of each size-fractioned particulate mercury (Hg^P) in the South China Sea (SCS) during our cruise.

Sampling time (Year/Month/Day)	Size range (μm)									Hg^P in PM$_{10}$
	< 0.4	0.4–0.7	0.7–1.1	1.1–2.1	2.1–3.3	3.3–4.7	4.7–5.8	5.8–9.0	9.0–10	
2015/9/4–6	3.03	1.69	2.90	2.47	2.04	1.72	1.55	1.46	1.39	24.35
2015/9/6–8	0.57	0.39	0.36	0.30	0.24	0.26	1.20	0.51	0.60	5.93
2015/9/8–10	0.67	0.65	0.48	0.88	0.52	1.04	0.89	0.49	0.50	8.15
2015/9/10–12	1.00	1.18	1.59	0.73	0.59	0.82	0.94	0.69	0.74	11.05
2015/9/15–17	0.33	0.21	0.45	0.18	0.41	0.50	0.50	0.74	0.60	5.23
2015/9/17–19	0.96	0.39	1.30	0.38	1.14	0.36	0.84	1.46	0.82	10.2
2015/9/19–21	0.46	0.32	0.13	0.49	0.29	0.34	0.29	1.13	0.41	5.15
2015/9/21–23	0.43	0.28	0.30	0.13	0.14	0.14	0.26	0.47	0.30	3.26
2015/9/23–25	0.97	0.68	1.02	1.15	0.99	0.88	0.89	0.92	0.82	11.09
2015/9/25–27	0.49	0.44	0.64	0.53	0.52	0.47	0.62	0.76	0.59	6.75
Average value	0.89	0.62	0.92	0.72	0.69	0.65	0.80	0.86	0.68	9.12

Table S2. The dry deposition flux (ng m^{-2} d^{-1}) of each size-fractioned Hg^P in the SCS during our cruise.

Sampling time (Year/Month/Day)	Size range (μm)									Total dry deposition
	< 0.4	0.4–0.7	0.7–1.1	1.1–2.1	2.1–3.3	3.3–4.7	4.7–5.8	5.8–9.0	9.0–10	
2015/9/4–6	0.0785	0.0146	0.0251	0.1280	0.2644	0.2229	0.2009	0.6938	0.6605	2.2887
2015/9/6–8	0.0148	0.0034	0.0031	0.0156	0.0311	0.0337	0.1555	0.2424	0.2851	0.7846
2015/9/8–10	0.0174	0.0056	0.0041	0.0456	0.0674	0.1348	0.1153	0.2328	0.2376	0.8607
2015/9/10–12	0.0259	0.0102	0.0137	0.0378	0.0765	0.1063	0.1218	0.3279	0.3516	1.0718
2015/9/15–17	0.0086	0.0018	0.0039	0.0093	0.0531	0.0648	0.0648	0.3516	0.2851	0.8431
2015/9/17–19	0.0249	0.0034	0.0112	0.0197	0.1477	0.0467	0.1089	0.6938	0.3897	1.4459
2015/9/19–21	0.0119	0.0028	0.0011	0.0254	0.0376	0.0441	0.0376	0.5370	0.1948	0.8923
2015/9/21–23	0.0111	0.0024	0.0026	0.0067	0.0181	0.0181	0.0337	0.2233	0.1426	0.4588
2015/9/23–25	0.0251	0.0059	0.0088	0.0596	0.1283	0.1140	0.1153	0.4372	0.3897	1.2840
2015/9/25–27	0.0127	0.0038	0.0055	0.0275	0.0674	0.0609	0.0804	0.3612	0.2804	0.8997
Average value	0.0231	0.0054	0.0079	0.0375	0.0892	0.0846	0.1034	0.4101	0.3217	1.0830

Table S3. Atmospheric GEM, surface seawater DGM and temperature (T_w), wind speed (u_{10}), saturation and
air-sea flux of Hg^0 during our cruise.

| Station	Position Longitude (°E)	Latitude (°N)	Date and time (Year/Month/Day/Local Time)	Depth m	DGM pg l⁻¹	PAR W m⁻²	GEM ng	T_w ℃	Wind speed m s⁻¹	Saturation %	Flux ng m⁻²
1	114.73	22.22	2015/09/05/10:15	44	57.8	152.19	1.86	27.3	7.3	1053	7.36
3	115.09	21.59	2015/09/06/04:15	94	41.4	0	1.16	29.2	7.8	1268	6.18
5	115.44	21.06	2015/09/06/08:10	123	37.0	86.76	1.33	29.2	7.3	993	4.73
8	115.63	20.64	2015/09/06/14:50	389	34.9	111.08	1.24	30.0	7.1	1021	4.26
10	115.81	20.33	2015/09/06/19:50	657	32.0	0	1.19	29.9	6.2	976	2.96
11	115.08	19.96	2015/09/07/14:50	960	30.4	88.62	1.26	30.2	5.4	881	2.11
13	114.90	20.28	2015/09/08/07:00	151	37.8	39.76	1.44	29.7	4.6	949	1.91
16	114.63	20.75	2015/09/08/15:30	85	33.0	21.35	2.37	29.7	7.5	501	3.97
18	114.36	21.23	2015/09/08/17:55	91	36.8	10.09	2.27	29.0	11.5	576	10.72
20	114.00	21.86	2015/09/08/23:25	33	66.8	0	2.39	26.4	5.0	927	3.91
21	113.28	21.49	2015/09/09/04:10	41	44.5	0	1.72	25.5	9.4	835	9.04
23	113.64	20.86	2015/09/09/08:50	91	37.5	76.89	2.09	28.8	10.6	630	9.42
26	113.93	20.33	2015/09/09/14:10	178	30.0	183.39	1.82	29.9	9.7	598	6.29
31	111.85	18.85	2015/09/10/06:40	343	33.8	7.02	1.86	30.0	6.2	661	2.96
34	111.49	19.06	2015/09/10/12:48	178	37.9	189.97	1.52	30.1	7.0	910	4.43
36	111.26	19.19	2015/09/10/16:10	108	40.4	110.82	1.46	30.2	7.3	1015	5.21
38	111.02	19.33	2015/09/10/19:50	25	55.9	0	1.49	30.1	8.2	1372	9.34
39	110.70	18.90	2015/09/10/22:50	14	65.9	0	1.64	30.2	3.7	1468	2.26
41	110.90	18.70	2015/09/11/03:10	20	41.0	0	1.58	30.1	6.8	947	4.54
44	111.20	18.40	2015/09/11/08:10	97	32.9	32.95	1.73	30.2	7.8	697	4.60
46	111.40	18.20	2015/09/11/13:00	1546	35.0	197.57	1.62	30.2	9.8	792	7.88
47	110.80	17.50	2015/09/11/20:00	1013	33.8	0	1.63	30.1	8.7	757	5.96
49	110.65	17.75	2015/09/12/02:20	664	35.6	0	1.80	30.1	5.7	723	2.67
52	110.43	18.13	2015/09/12/10:35	95	41.2	169.76	1.69	30.0	7.8	891	5.97
54	110.28	18.38	2015/09/12/14:10	15	58.9	183.59	1.57	30.3	8.9	1373	11.61
62	110.50	15.45	2015/09/17/00:10	613	46.6	0	1.82	27.9	6.6	882	4.77
60	111.50	15.45	2015/09/17/18:40	1281	29.7	0	1.12	28.9	6.3	940	2.80
57	113.00	15.45	2015/09/18/08:10	2847	24.1	41.78	1.49	29.9	4.0	587	0.86
55	113.95	15.25	2015/09/18/15:55	1073	27.9	139.61	1.38	30.3	4.4	741	1.25
73	114.00	14.00	2015/09/18/22:30	4356	34.9	0	1.37	29.9	8.5	926	6.02
71	113.00	14.00	2015/09/19/06:00	2513	30.3	3.87	1.22	29.9	6.1	904	2.68
69	112.00	14.00	2015/09/19/13:00	1803	36.7	195.05	1.12	29.7	5.4	1182	2.62
68	111.50	14.00	2015/09/19/19:10	2773	32.1	0	1.08	29.9	6.3	1082	3.10
65	110.50	14.00	2015/09/20/06:00	1951	23.0	0	1.52	29.2	3.4	537	0.58
81	110.50	13.00	2015/09/20/13:45	2546	30.5	200.23	1.40	29.8	5.5	791	2.16
79	111.50	13.00	2015/09/21/01:30	2333	38.0	0	1.98	29.9	4.2	696	1.54
76	113.00	13.00	2015/09/21/13:50	4033	34.9	165.63	1.37	29.4	3.5	916	1.02
74	114.00	13.00	2015/09/21/21:30	4243	32.1	0	1.31	29.9	2.3	892	0.40
90	114.00	12.00	2015/09/22/08:50	4349	34.7	77.65	1.60	29.9	4.4	789	1.57
107	114.00	11.00	2015/09/22/15:55	3387	36.1	115.95	1.58	29.4	5.1	819	2.20
109	113.50	10.00	2015/09/23/00:30	3050	38.6	0	1.28	29.5	6.9	1085	4.46
111	112.50	10.00	2015/09/23/18:30	1814	29.6	5.12	1.36	29.7	7.2	785	3.58
112	112.00	10.00	2015/09/24/16:40	2357	37.0	33.50	1.48	29.7	10.2	899	9.15
113	111.50	10.00	2015/09/24/20:20	3347	29.2	0	1.44	29.6	9.9	733	6.61
114	111.00	10.00	2015/09/25/00:30	3372	34.8	0	1.46	29.4	10.6	852	9.22
115	110.50	10.00	2015/09/25/05:30	2533	31.5	0	1.46	29.3	11.2	771	9.19
100	110.50	10.50	2015/09/25/08:00	1791	37.1	77.25	1.37	29.3	11.5	966	11.75
99	110.50	11.00	2015/09/25/14:15	1721	38.1	139.76	1.20	29.7	11.7	1140	12.71
102	111.50	11.00	2015/09/25/21:15	3853	35.7	0	1.24	29.7	11.7	1043	11.83
104	112.50	11.00	2015/09/26/05:40	4182	27.0	0	1.22	29.5	11.3	794	8.06
105	113.00	11.00	2015/09/26/08:20	4227	30.4	51.68	1.23	29.6	4.7	888	1.59
92	113.00	12.00	2015/09/26/14:20	4277	38.5	159.27	1.24	30.0	7.3	1134	5.01
94	112.00	12.00	2015/09/27/00:25	4281	31.3	0	1.26	30.1	7.5	908	4.20
96	111.00	12.00	2015/09/27/07:00	2256	34.6	11.87	1.25	29.9	5.8	1002	2.81
97	110.50	12.00	2015/09/27/11:00	2404	40.8	181.18	1.27	30.0	2.2	1171	0.48

58
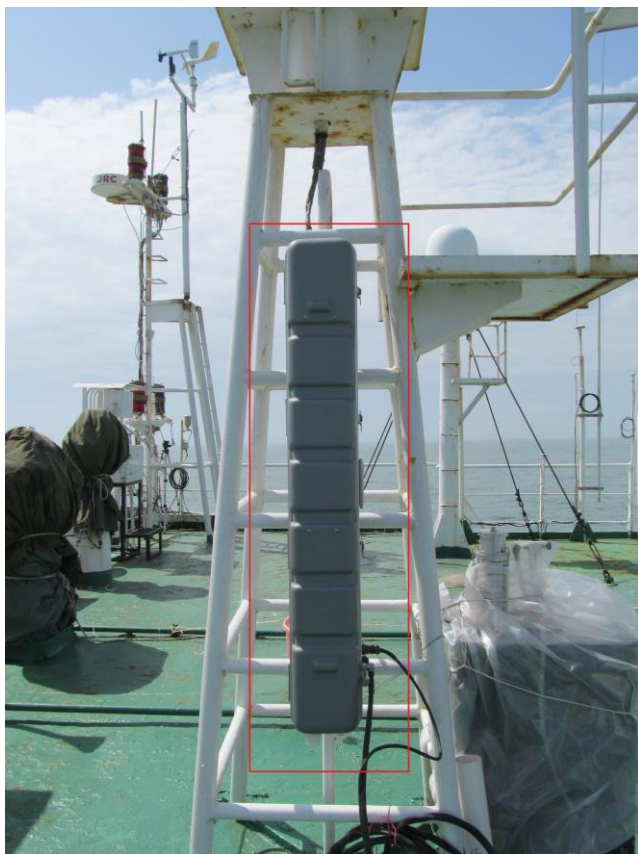
59 **Figure S1.** The insulated box of the RGM and Hg$^P_{2.5}$ sampling unit.
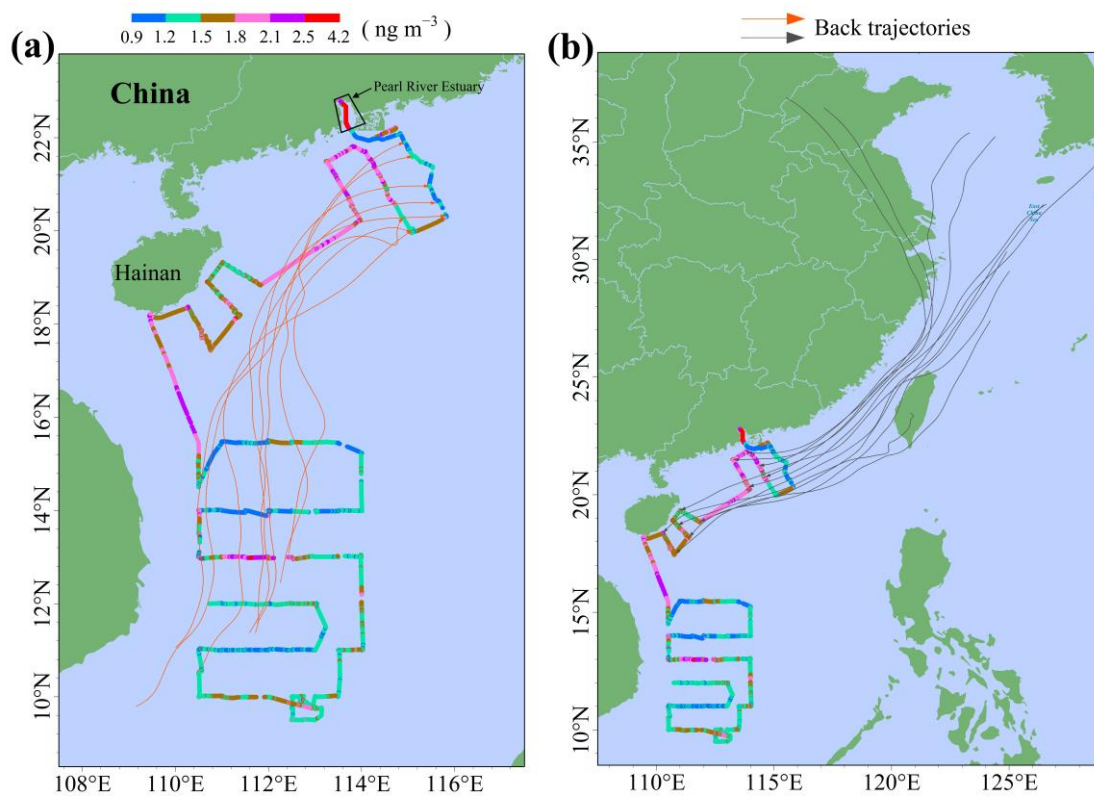

60

61 **Figure S2.** GEM concentrations over the northern SCS and 72-h back-trajectories arriving at some stations.
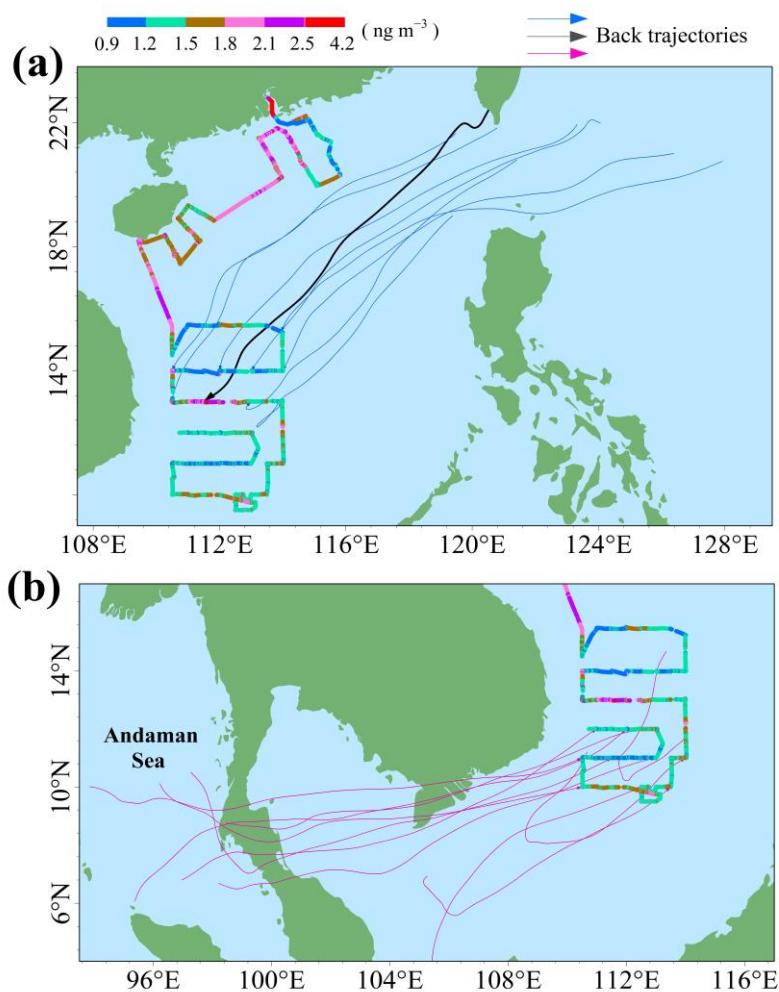
62

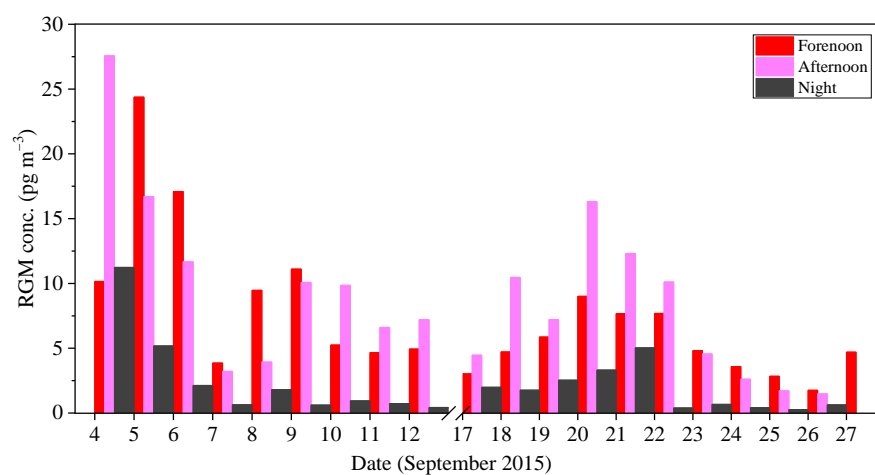**Figure S3.** GEM concentrations over the western SCS and 72-h back-trajectories arriving at some stations.

64

Figure S4. RGM concentrations in the forenoon, afternoon and night.